



저작자표시-비영리-변경금지 2.0 대한민국

이용자는 아래의 조건을 따르는 경우에 한하여 자유롭게

- 이 저작물을 복제, 배포, 전송, 전시, 공연 및 방송할 수 있습니다.

다음과 같은 조건을 따라야 합니다:



저작자표시. 귀하는 원저작자를 표시하여야 합니다.



비영리. 귀하는 이 저작물을 영리 목적으로 이용할 수 없습니다.



변경금지. 귀하는 이 저작물을 개작, 변형 또는 가공할 수 없습니다.

- 귀하는, 이 저작물의 재이용이나 배포의 경우, 이 저작물에 적용된 이용허락조건을 명확하게 나타내어야 합니다.
- 저작권자로부터 별도의 허가를 받으면 이러한 조건들은 적용되지 않습니다.

저작권법에 따른 이용자의 권리는 위의 내용에 의하여 영향을 받지 않습니다.

이것은 [이용허락규약\(Legal Code\)](#)을 이해하기 쉽게 요약한 것입니다.

[Disclaimer](#)

이학박사 학위논문

**Dynamics of transcription and transport of
Arc mRNAs in live neurons**

살아있는 뉴런에서의 Arc mRNA
전사과정과 움직임에 대한 연구

2020년 7월

서울대학교 대학원

물리천문학부

문형석

Ph.D. Dissertation

**Dynamics of transcription and transport of
Arc mRNAs in live neurons**

Hyungseok Moon

Supervised by

Professor Hye Yoon Park

July 2020

Department of Physics and Astronomy

Graduate School

Seoul National University

Abstract

Dynamics of transcription and transport of Arc mRNAs in live neurons

Hyungseok Moon

Department of Physics and Astronomy

Seoul National University

RNA is not just an intermediate product in the process of gene expression but has its role especially in introducing asymmetry to biological systems. The invention of RNA fluorescence in situ hybridization (FISH) led to numerous discoveries about RNA's new aspect as an active player in biological phenomena. Especially inside brain or network of neurons, the asymmetric expression of genes involved in synaptic plasticity is critical for the proper formation of a memory. In this regard, an immediate-early gene (IEG) Arc has been a key molecule for understanding the mechanism of memory consolidation since its discovery in 1995.

Arc is an IEG that is rapidly and transiently transcribed after strong neural activity. This property has been used to evaluate which group of neurons underwent neural activity during various behavioral studies. Surprisingly after transcription, Arc

mRNA was reported to localize near highly activated synapses. Arc is one of the special few genes which undergoes both neural activity-dependent transcription and localization of its mRNA to the activated synapses. However, these two phenomena were investigated by the FISH method which needs chemical fixation of the sample and thus the information about its dynamics was inaccessible. To overcome this problem, we've generated Arc-PBS mouse and was successful in real-time imaging of Arc mRNA transcription and transport in the live neuron at single-molecule resolution.

In this study, we generated Arc-PBS mouse in which tandem repeats of PBS sequences are knocked in the 3' untranslated region (UTR) of Arc genetic locus. By performing FISH and western blot, we confirmed PBS knock in on Arc 3' UTR doesn't alter the Arc mRNA and protein expression level. Next, we investigated the correlation between Ca^{2+} activity and Arc transcription which is often believed to be in the relation of one to one correspondence. By directly measuring somatic Ca^{2+} spikes and Arc transcription from the same neuron for the first time, we observed only ~43 % of neurons transcribed Arc mRNA even after somatic Ca^{2+} bursts in dissociated hippocampal neuron culture. Afterwards, by performing combined immunofluorescence with FISH, we showed phosphorylated CREB level has a positive correlation with Arc transcription suggesting that the ability to induce the Arc transcription might vary from neuron to neuron depending on their internal states. Finally, we observed the real-time transport dynamics of endogenous Arc

mRNAs in the dendrite for the first time. The directed transport of Arc mRNA occurred in both anterograde and retrograde directions and was often interrupted by long pauses similar to the previously reported transport behavior of β -actin mRNA. The effect of neural activity on velocity, the occurrence of run in the anterograde or retrograde direction, and the portion of moving Arc mRNAs was assessed. Surprisingly, none of these parameters were affected by global inhibition of ionotropic neural activity suggesting mechanism that makes Arc mRNA localize to activated synapses is different from that of mitochondria.

Collectively, in this thesis, we first demonstrate the real-time single-molecule dynamics of endogenous Arc mRNA transcription and dendritic transport in live neurons. We could measure quantities that were impossible or extremely challenging to obtain by traditional fixed cell approaches. This innovative approach of imaging Arc mRNA in live neurons would help us elucidate the mechanism of memory consolidation by revealing its dynamic aspects.

Keywords: Arc mRNA, transcription, RNA localization, dendritic transport, single-molecule imaging, live-cell imaging

Student Number: 2014-22365

Table of Contents

LIST OF FIGURES AND TABLES.....	VIII
1. INTRODUCTION	1
1.1. Gene <i>Arc</i>	1
1.2 RNA imaging method	3
1.3 Biological system: Primary neuron culture	6
1.4 Imaging system: Widefield microscope.....	7
1.5 References.....	9
2. GENERATION OF ARC-PBS MOUSE	14
2.1 Introduction.....	14
2.2 Materials and Methods.....	16
2.3 Results and Discussion	23
2.4 References.....	28
3. CA²⁺ ACTIVITY AND ARC TRANSCRIPTION.....	30
3.1 Introduction.....	30
3.2 Materials and Methods.....	33
3.3 Results and Discussion	39
3.4 Conclusion and Outlook.....	52
3.5 References.....	54

4. DYNAMICS OF ARC MRNA TRANSPORT IN DENDRITE OF LIVE HIPPOCAMPAL NEURONS.....	57
4.1 Introduction	57
4.2 Materials and Methods.....	60
4.3 Results and Discussion	63
4.4 Conclusion and outlook.....	70
4.5 References.....	73
5. CONCLUSION AND OUTLOOK.....	79
ABSTRACT IN KOREAN (국문초록).....	82

List of Figures and Tables

Figure 1.1. RNA labeling techniques (A) Fluorescence in situ hybridization (FISH). Usually 20-mer or 50-mer oligonucleotides are used for FISH probes, but for convenience, FISH probes are illustrated as 4-mer oligonucleotide here. (B) PP7 system. PCP-GFP must dimerize before binding to single PBS stem-loop. The caveat is PCP-GFP level must be high in order to form enough PCP-GFP dimers. But this high PCP-GFP level increases the background signal of unbound PCP-GFPs. Therefore, stdPCPstdGFP construct is widely used these days (std stands for synonymous tandem mutation). Due to the linker, this construct undergoes efficient intramolecular dimerization enabling efficient binding to stem-loops even in low concentration.

Figure 1.2 Maturation of neuron culture in vitro (A) DIV 1 (B) DIV 3 (C) DIV 15

Figure 1.3 Schematics of widefield microscope

Figure 2.1 Schematics of the endogenous Arc locus, Arc-PBS targeting construct, and the final targeted locus.

Figure 2.2 Arc transcriptional output is not altered by PP7 knock-in. (A) Representative image of neurons with Arc transcription sites from Arc-PBS KI heterozygous x heterozygous cultured neurons. PBS-LK Quasar570 (Green) and Arc-CDS Quasar670 probe (Red). Yellow transcription sites are PBS knocked in alleles whereas red transcription sites are wildtype transcription sites. (B) Scatter plot of nascent mRNA numbers at Arc-PBS knocked-in transcription sites by LK 20 mer FISH versus Arc CDS FISH. (n= 17). PBS stem-loop signal reliably recapitulates Arc transcription activity. (C) Average nascent mRNA numbers of untagged allele and tagged allele determined by Arc CDS FISH. Error bars represent standard deviation. (n=18 for untagged alleles, n=17 for tagged alleles.)

Figure 2.3 Comparison of homozygous Arc-PBS mouse to WT mouse. (A) Western blot image of Arc protein (55 kDa) and GAPDH protein (36 kDa) in brain tissue lysates from three WT (Arc^{+/+}) and three homozygous Arc-PBS (Arc^{P/P}) knock-in mice (upper panel). (B) Two nonspecific bands were produced by nonspecific binding of secondary antibody. (C) Relative Arc expression quantified using GAPDH as loading control was compared between WT and Arc^{P/P} mice (lower panel). No significant difference was observed ($P > 0.05$, $n = 3$ mice). Error bars represent standard deviation (SD).

Figure 3.1 Synchronized Ca²⁺ activity during bicuculline incubation. (A) GFP channel image showing AAV-hSyn-NLS-tdPCP-tdGFP infected neurons (DIV 14) were imaged using a 20× magnification objective. (B) Somas of GFP positive neurons were selected to be analyzed. (C) Cy3 channel image showing Calcium Orange stained neurons. (D) Synchronized Ca²⁺ activities induced by 50 μM bicuculline incubation. Most of neurons showed synchronized Ca²⁺ spikes. (E) Ca²⁺ burst frequency change during bicuculline stimulation ($n = 46$ neurons from 2 different cultures). Error bars represent SD.

Figure 3.2 Persistent synchronized Ca²⁺ activities after bicuculline washout. (A) GFP channel image showing AAV-hSyn-NLS-tdPCP-tdGFP infected neurons (DIV 10) imaged using a 20× magnification objective. (B) Somas of GFP positive neurons were selected to be analyzed. (C) Cy3 channel image showing Calcium Orange stained neurons. (D) Synchronized Ca²⁺ activities 20 min after washout of bicuculline. (E) Synchronized Ca²⁺ activities 60 min after washout of bicuculline.

Figure 3.3 Tagging of Arc transcription sites by tdPCP-tdGFP (A) Schematic of Arc DNA and Arc mRNA from Arc-PBS mouse. (B) Tagging of endogenous Arc mRNA by exogenous PCP-GFP expression. (C) Arc transcription site visualized by linker targeting FISH probes (Q570). (D) Arc transcription site visualized by tdPCP-tdGFP tagging. (E) DAPI stained nucleus. (F) Composite image of 3

channels. FISH (Red), tdPCP-tdGFP (Green), and DAPI (Blue). Scale bar represents 10 μm .

Figure 3.4 Blinking of Arc transcription. (A) Time-lapse images of Arc transcription. Scale bar represents 5 μm . (B) Time-course of Arc transcriptional activity was analyzed by custom matlab program. 2D gaussian fitted amplitude of transcription site was used to describe Arc transcription activity of each allele.

Figure 3.5 Ca^{2+} activity and Arc transcription from live neurons were observed by dual-color imaging. (A) Experiment scheme of imaging both Ca^{2+} activity and Arc transcription from the same neuron. One green block represents one z-stack imaging through the nucleus to detect Arc transcription sites in the GFP channel. One red block represents continuous Ca^{2+} activity imaging at the single plane of the nucleus for ~5 min in the Cy3 channel. The same neuron was monitored before and after the stimulation by 50 μM bicuculline. (B) Representative Ca^{2+} activity snapshot from the Cy3 channel. (C) Synchronized Ca^{2+} activities measured from the soma (area within dashed line) of neuron 1 (upper panel) and neuron 2 (lower panel) 5 min after bicuculline stimulation. (D) Representative image of Arc transcription snap shot in the same neurons as shown in (B). Transcription from both alleles in neuron 1 (cyan and magenta arrow heads) versus no transcription from neither allele in neuron 2. (E) Time-course plot of Arc transcription activity in neuron 1 (upper panel) and neuron 2 (lower panel).

Figure 3.6 Plot of Ca^{2+} activity and Arc transcription activities. Data set of neurons with Arc transcription. First column represents Ca^{2+} activity before stimulation (basal condition). Second column represents Ca^{2+} activity within 5 min after bicuculline application except for neuron 19. In case of neuron 19, Ca^{2+} activity of second column was measured 7-10.5 min after stimulation. Therefore, Arc transcription image for neuron 19 was taken from 11 min after stimulation. Third column represents Ca^{2+} activity 28-33 min after stimulation. The last column

corresponds to time-lapse Arc transcription activity during 5-27 min after stimulation.

Figure 3.7 Heterogenous distribution of initiation and duration of Arc transcription bursts. (A) Distribution of first initiation time of Arc transcription after bicuculline stimulation (n=22 transcription sites). (B) Distribution of Arc transcriptional burst duration after bicuculline stimulation (n=9 transcription sites).

Figure 3.8 Comparison of somatic Ca²⁺ spikes between two groups of neurons with or without Arc transcription within 30 min after bicuculline stimulation. (A) Comparison of the average full width at half maximum (FWHM) of Ca²⁺ spikes. No significant difference was observed between two groups ($P_{ks} > 0.05$, Kolmogorov –Smirnov test). (B) Comparison of average burst frequency of Ca²⁺ spikes. No significant difference was observed between two groups ($P_{ks} > 0.05$, Kolmogorov –Smirnov test). Error bars represent SD (n = 20 neurons for Arc transcription ON group, and n = 26 neurons for Arc transcription OFF group).

Figure 3.9 Neurons with high pCREB levels have high probability of having Arc transcription sites. (A) Representative IF-smFISH image of Arc transcription (green) and phosphorylated CREB (red) in the nucleus (DAPI, blue). Scale bar represents 10 μ m. (B) Probability of having Arc transcription sites. Neurons were grouped by pCREB levels in the nucleus. (**, $P < 0.01$; *, $P < 0.05$; Two-tailed t-test). Total of 203 neurons were imaged from four independent experiments. Error bars represent SEM.

Figure 4.1 Selective localization of Arc mRNA to activated synapses. This figure summarizes one of key findings of reference [4.1]. LTP inducing high frequency stimulus was given to yellow neuron (Here, only axon part of yellow neuron is shown.). Arc mRNAs are induced from purple neuron as purple neuron gets excited by receiving inputs from synapses with yellow neuron. After continuous delivery of stimulation for 2 hours, Arc mRNAs are localized near highly activated synapse

between purple and yellow neurons.

Figure 4.2 False positive tdPCP-tdGFP aggregates in dendrite. (A) A representative image of false positive particles in dendrite from tdPCP-tdGFP infected wild-type neuron. (B) A representative image of dendrite from stdPCP-stdGFP infected wild-type neuron. False particles are not observed. (C) Fraction of moving particles during 1 min observation in basal condition (Base) and bicuculline stimulated condition (Bicu). (D) Probability distributions of speed of run phase in basal condition (cyan) and bicuculline stimulated condition (orange). (C) and (D) were analyzed from tdPCP-tdGFP infected Arc^{p/p} homozygous neuron culture which real Arc mRNAs and false positive particles are both present due to tdPCP-tdGFP aggregates. Scale bar represents 5 μ m. Total of 1580 particles for bicuculline stimulated condition and 1454 particles from basal condition were analyzed from 5 independent experiments.

Figure 4.3 Tagged endogenous Arc mRNA localizes near dendritic spines. A representative image of Arc mRNAs localized at the neck of a dendritic spine (upper right panel) and inside a spine (lower right panel).

Figure 4.4 Representative kymograph of Arc mRNAs in dendrite. Both stationary and actively moving Arc mRNAs are present in a dendrite. In this figure, nucleus is at the left side and not shown. Thus, Arc mRNA's run toward left direction is retrograde motion and toward right direction is anterograde direction. Constant velocity motion can be frequently observed.

Figure 4.5 Transport dynamics of dendritic Arc mRNA. (A) Fraction of moving Arc mRNAs that displacement is more than 1.5 μ m during 1 min of observation after bicuculline (Bic) and KCl stimulation (KCl). 510 and 141 mRNAs were analyzed for Bic and KCl conditions, respectively. (B) Fraction of moving Arc mRNAs in the bicuculline washout (Control), bicuculline washout + TTX (TTX) condition and bicuculline washout + TTX + APV + CNQX (TTX + APV + CNQX).

510, 427, and 549 mRNAs were analyzed for Control, TTX and TTX + APV + CNQX conditions, respectively. (C) Probability density function (PDF) of the velocity in Control (yellow), TTX (blue) and TTX + APV + CNQX (red) conditions, respectively. Velocity of run of Arc mRNA was similar among all conditions. (D) Percentage of anterograde (antero) and retrograde (retro) runs in all conditions. (E) Histogram of distance traveled by a single run movement in anterograde and retrograde directions for Control, TTX, and TTX + APV + CNQX conditions, respectively. (*, $P < 0.05$; Two-tailed t-test). For (B)-(E), total of 173, 146 and 212 runs from 5 independent experiments were analyzed for Control, TTX and TTX + APV + CNQX conditions, respectively. Error bars represent SEM.

Table 1. Sequence of the probes used for smFISH against the Arc coding sequence (CDS) and linker sequence (LK). Arc CDS Probe sets are modified at 3'ends for conjugation to Quasar 670. LK probes sets are modified at both 5' and 3'ends. CDS probes are labeled with Quasar 670 (Biosearch) and LK probes are labeled with Quasar 570 (Biosearch).

Table 2. Sequence of the probes used for smFISH against the Arc coding sequence (CDS). Probe sets are modified at both 5' and 3'ends for conjugation to dye of choice. CDS probes are labeled with Quasar 570 (Biosearch).

Table 3. Previously measured speeds of motor proteins

1. Introduction

1.1. Gene *Arc*

1.1.1. Arc protein

Arc/Arg3.1 (activity-regulated cytoskeleton-associated protein/activity-regulated gene 3.1) is a single copy gene specifically expressed at testis and brain [1-3]. Unlike other immediate early genes (IEG) which are usually transcription factors, Arc is a cytosolic protein which is involved in the endocytosis of AMPA receptors [4, 5]. Not only important for decreasing the synaptic strength or long-term depression (LTD), Arc protein was also known to be involved in the process of increasing the synaptic strength by long-term potentiation (LTP) [5, 6]. However, function of Arc in the LTP is controversial. There is a recent report persuading that Arc is not required for the induction of LTP [7]. With these two features of Arc (1. Neural activity responsive IEG 2. Involved in LTD) combined, Arc can regulate homeostatic synaptic scaling [8]. Changing synaptic strength is critical for the

formation of the memory. Therefore, Arc knockout mouse exhibits impaired long term memory formation [6]. Strikingly, recent research suggests that Arc protein can oligomerize and form viral like capsid protein to mediate cell to cell communication [9, 10]. However, the actual function of these Arc exosomes are not well known yet.

1.1.2. Arc mRNA

Arc mRNA transcription happens rapidly upon neural stimulation [1, 2]. Therefore transcription of Arc has been used as a marker for activated neurons with time delay of about ~10 min [11]. This is very useful for observing activity pattern of the deep brain parts in cellular resolution where Ca^{2+} imaging is inaccessible. Synaptic activity-responsive element (SARE) present at ~7kb upstream of transcription initiation site mediates the neural activity dependent induction of Arc transcription [12]. Also, nuclear Ca^{2+} spikes has been suggested to be important factor for the fast induction of IEG transcription [13]. Another interesting feature of Arc is that Arc mRNA localizes to highly activated synapses and undergoes local translation in response to neural activity [14, 15]. These features of Arc made neuroscientists consider Arc as a master molecule of synaptic plasticity.

1.2 RNA imaging method

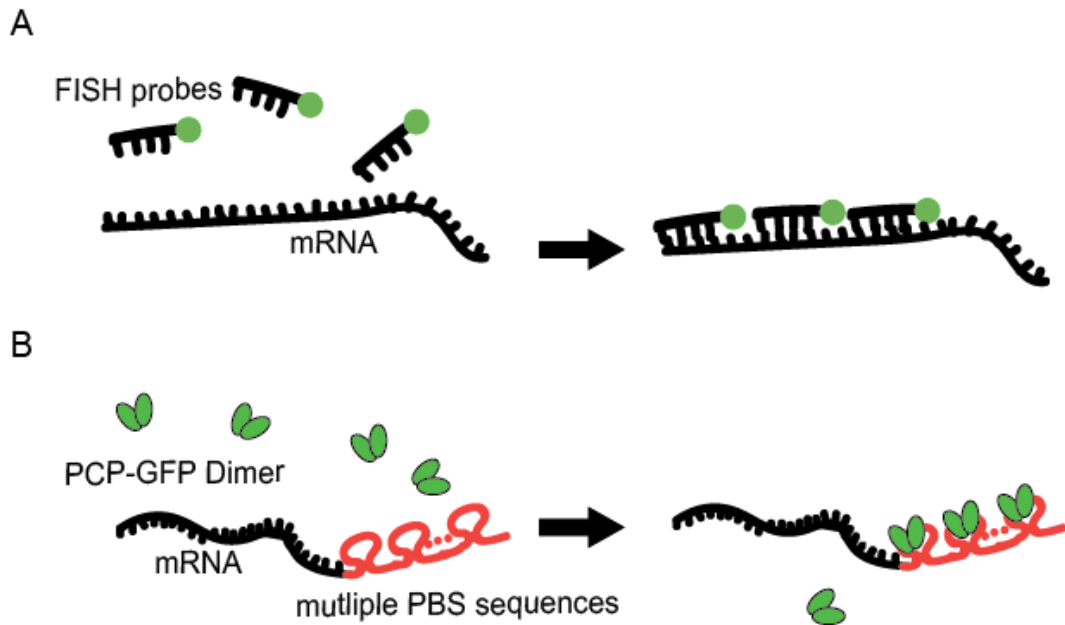


Figure 1.1. RNA labeling techniques

(A) Fluorescence in situ hybridization (FISH). Usually 20-mer or 50-mer oligonucleotides are used for FISH probes, but for convenience, FISH probes are illustrated as 4-mer oligonucleotide here. (B) PP7 system. PCP-GFP must dimerize before binding to single PBS stem-loop. The caveat is that PCP-GFP level must be high in order to form sufficient PCP-GFP dimers. But this high PCP-GFP level increases the background signal of unbound PCP-GFPs. Therefore, stdPCP-stdGFP construct is widely used these days ('std' stands for synonymous tandem mutation). Due to the linker, this construct undergoes efficient intramolecular dimerization enabling efficient binding to stem-loops

even in low concentration or background [27].

1.2.1. Fluorescence in situ hybridization (FISH)

FISH is the most widespread method for visualizing specific target RNA with cellular contexts preserved [16]. Fluorescently labelled hybridizing probes with complementary sequences to target mRNA are used for the detection of target gene (Figure 1.1A). In order to observe mRNA in single molecule resolution, usually ~20 of 20-mer probes with 2 dyes labeled at the both ends are used. These days, a lot of more sophisticated techniques which have their own strengths were developed including RNAscope, seqFISH, merFISH, etc [17, 18, 19]. FISH can also be combined with immunofluorescence (FISH-IF) enabling observation of both protein and mRNA together [20]. However, in situ hybridization needs chemical fixation of the sample.

1.2.2. MS2 based systems

Escherichia virus MS2 is a single-stranded RNA virus that infects bacteria [21]. The MS2 coat protein (MCP) dimer binds to its partner RNA MS2 binding site (MBS) with high affinity in sequence specific manner [22]. In 2001, Dr.Singer's lab first demonstrated that this RNA-protein pair can be used to visualize mRNA in living yeast [23]. In principle, MS2 stem-loops are knocked in the untranslated region of

mRNA to not disturb the translation of the gene. And paired with that, Fluorescent protein linked MCP are expressed together. Usually, nucleus localization sequence (NLS) is also attached. There are two advantages by doing so. First, NLS provides enough MCP concentration to immediately tag mRNA of interest enabling the observation of transcription inside nucleus. Second, NLS provides less background at the cytoplasm of the cell, enabling mRNA observation at the cytosol in single molecule resolution. This MS2 system was applied to generate transgenic mouse that labels all the β -actin mRNAs [24, 25]. This pioneering work enabled visualization of β -actin transcription sites in brain slices and dendritic transport dynamics of β -actin mRNAs. This further lead to the discovery of random walk model that nicely describes dendritic transport dynamics of β -actin mRNAs for the first time. There is another similar RNA-protein pair from Bacteriophage PP7 which has minimal crosstalk with MS2 system (Figure 1.1B). This can facilitate simultaneous mRNA imaging of two different genes [26].

1.3 Biological system: Primary neuron culture

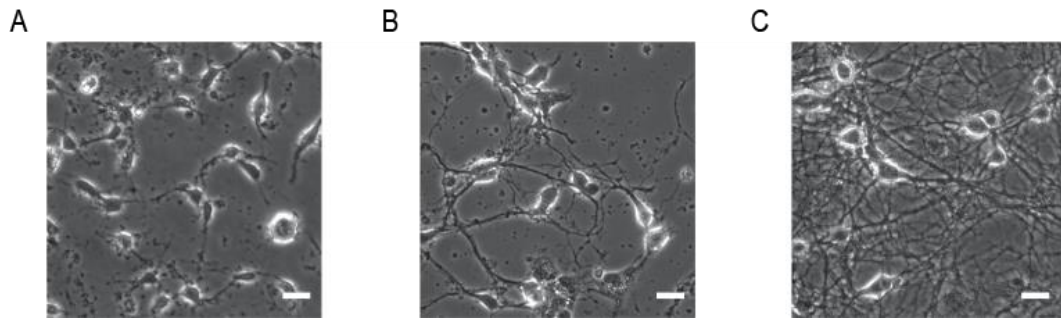


Figure 1.2 Maturation of neuron culture in vitro

(A) DIV 1 (B) DIV 3 (C) DIV 15

Since the first observation of live cultured neuron at 1910 by Dr. Harrison, primary neuron culture system has significantly evolved our understanding of brain system [28]. As neurons don't undergo cell division, neuron culture has life span. In our culturing condition, life span of neuron culture was typically up to a month [29]. Primary neuron culture system has critical disadvantages of losing original circuit and neurons grown *in vitro* might have some physiological difference from neurons inside the actual brain. However compared to *in vivo*, it is much easier to manipulate primary neuron culture by chemicals or electricity. And primary neuron culture permits imaging experiments that need high magnification such as super resolution imaging or single molecule imaging as neurons are grown on fine coverslips. Most of the experiments on this study were performed on ~ DIV 14 neurons when synapses are matured and Arc expression level is sufficient.

1.4 Imaging system: Widefield microscope

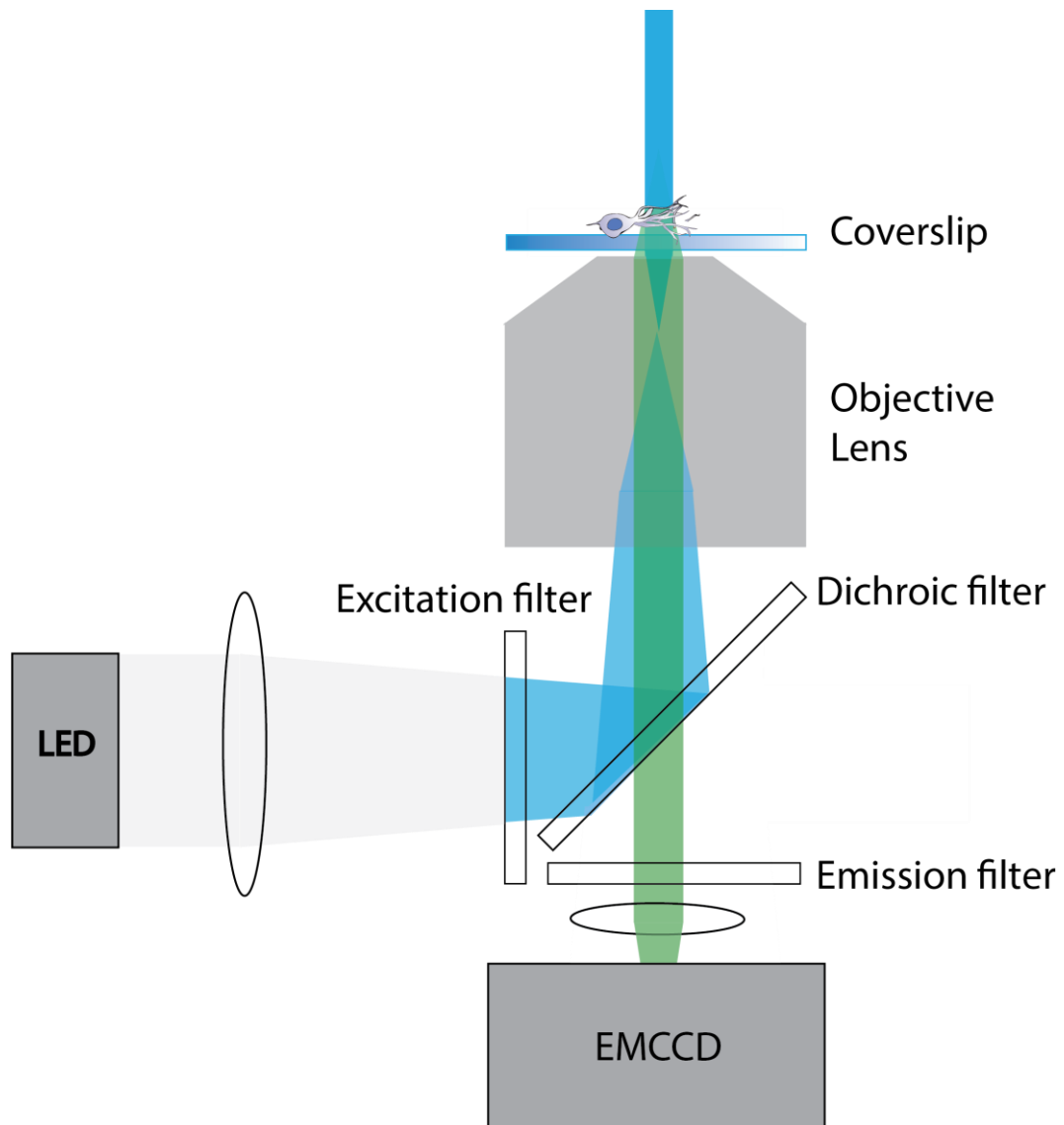


Figure 1.3 Schematics of widefield microscope

Widefield microscope is conventionally used microscope which collimated beam from laser or LED illuminate the sample. In our lab, we've used white LED with

liquid light guide collimator as an excitation source. Various lasers with different wavelengths can be also used as an excitation source for widefield microscope. One disadvantage of white LED or argon lamp is that sometimes excitation spectra cannot be completely separated by excitation filter resulting in some bleed-through between two channels. This becomes critical especially when the signal intensity difference between two channels is large. For example, smFISH signals are usually weak, but IF signals are too strong. In this case, bleed-through can happen from IF channel to smFISH channel. Compared to confocal microscope, widefield microscope is not point scanning. Therefore, its frame rate can be faster and exposure time per pixel can be longer when compared to confocal microscope. Also, widefield microscope collects all signal from out of focus z planes whereas confocal microscope facilitates pinhole to block signal from other z planes. In case of single layered cell culture, we found out widefield microscope with high NA objective lens and EMCCD is better for imaging mRNA in single molecule resolution compared to confocal microscope.

1.5 References

1. Link, W., Konietzko, U. W. E., Kauselmann, G., Krug, M., Schwanke, B., Frey, U., & Kuhl, D. (1995). Somatodendritic expression of an immediate early gene is regulated by synaptic activity. *Proceedings of the National Academy of Sciences*, 92(12), 5734-5738.
2. Lyford, G. L., Yamagata, K., Kaufmann, W. E., Barnes, C. A., Sanders, L. K., Copeland, N. G., ... & Worley, P. F. (1995). Arc, a growth factor and activity-regulated gene, encodes a novel cytoskeleton-associated protein that is enriched in neuronal dendrites. *Neuron*, 14(2), 433-445.
3. Maier, B., Medrano, S., Sleight, S. B., Visconti, P. E., & Scrabble, H. (2003). Developmental association of the synaptic activity-regulated protein arc with the mouse acrosomal organelle and the sperm tail. *Biology of reproduction*, 68(1), 67-76.
4. Waung, M. W., Pfeiffer, B. E., Nosyreva, E. D., Ronesi, J. A., & Huber, K. M. (2008). Rapid translation of Arc/Arg3.1 selectively mediates mGluR-dependent LTD through persistent increases in AMPAR endocytosis rate. *Neuron*, 59(1), 84-97.
5. Chowdhury, S., Shepherd, J. D., Okuno, H., Lyford, G., Petralia, R. S., Plath, N., ... & Worley, P. F. (2006). Arc/Arg3.1 interacts with the endocytic machinery to regulate AMPA receptor trafficking. *Neuron*, 52(3), 445-459.
6. Plath, N., Ohana, O., Dammermann, B., Errington, M. L., Schmitz, D., Gross, C., ... & Kobalz, U. (2006). Arc/Arg3.1 is essential for the

- consolidation of synaptic plasticity and memories. *Neuron*, 52(3), 437-444.
7. Kyrke-Smith, M., Volk, L. J., Cooke, S. F., Bear, M. F., Huganir, R. L., & Shepherd, J. D. (2020). The immediate early gene Arc is not required for hippocampal long-term potentiation. *bioRxiv*.
 8. Shepherd, J. D., Rumbaugh, G., Wu, J., Chowdhury, S., Plath, N., Kuhl, D., ... & Worley, P. F. (2006). Arc/Arg3.1 mediates homeostatic synaptic scaling of AMPA receptors. *Neuron*, 52(3), 475-484.
 9. Pastuzyn, E. D., Day, C. E., Kearns, R. B., Kyrke-Smith, M., Taibi, A. V., McCormick, J., ... & Briggs, J. A. (2018). The neuronal gene arc encodes a repurposed retrotransposon gag protein that mediates intercellular RNA transfer. *Cell*, 172(1-2), 275-288.
 10. Ashley, J., Cordy, B., Lucia, D., Fradkin, L. G., Budnik, V., & Thomson, T. (2018). Retrovirus-like Gag protein Arc1 binds RNA and traffics across synaptic boutons. *Cell*, 172(1-2), 262-274.
 11. Guzowski, J. F., McNaughton, B. L., Barnes, C. A., & Worley, P. F. (1999). Environment-specific expression of the immediate-early gene Arc in hippocampal neuronal ensembles. *Nature neuroscience*, 2(12), 1120-1124.
 12. Kawashima, T., Okuno, H., Nonaka, M., Adachi-Morishima, A., Kyo, N., Okamura, M., ... & Bitto, H. (2009). Synaptic activity-responsive element in the Arc/Arg3.1 promoter essential for synapse-to-nucleus signaling in activated neurons. *Proceedings of the National Academy of Sciences*, 106(1), 316-321.
 13. Hardingham, G. E., Arnold, F. J., & Bading, H. (2001). Nuclear

calcium signaling controls CREB-mediated gene expression triggered by synaptic activity. *Nature neuroscience*, 4(3), 261-267.

- 14. Steward, O., Wallace, C. S., Lyford, G. L., & Worley, P. F. (1998). Synaptic activation causes the mRNA for the IEG Arc to localize selectively near activated postsynaptic sites on dendrites. *Neuron*, 21(4), 741-751.**
- 15. Na, Y., Park, S., Lee, C., Kim, D. K., Park, J. M., Sockanathan, S., ... & Worley, P. F. (2016). Real-time imaging reveals properties of glutamate-induced Arc/Arg 3.1 translation in neuronal dendrites. *Neuron*, 91(3), 561-573.**
- 16. Singer, R. H., & Ward, D. C. (1982). Actin gene expression visualized in chicken muscle tissue culture by using in situ hybridization with a biotinated nucleotide analog. *Proceedings of the National Academy of Sciences*, 79(23), 7331-7335.**
- 17. Wang, F., Flanagan, J., Su, N., Wang, L. C., Bui, S., Nielson, A., ... & Luo, Y. (2012). RNAscope: a novel in situ RNA analysis platform for formalin-fixed, paraffin-embedded tissues. *The Journal of Molecular Diagnostics*, 14(1), 22-29.**
- 18. Lubeck, E., Coskun, A. F., Zhiyentayev, T., Ahmad, M., & Cai, L. (2014). Single-cell in situ RNA profiling by sequential hybridization. *Nature methods*, 11(4), 360.**
- 19. Chen, K. H., Boettiger, A. N., Moffitt, J. R., Wang, S., & Zhuang, X. (2015). Spatially resolved, highly multiplexed RNA profiling in single cells. *Science*, 348(6233), aaa6090.**
- 20. Eliscovich, C., Shenoy, S. M., & Singer, R. H. (2017). Imaging mRNA**

and protein interactions within neurons. *Proceedings of the National Academy of Sciences*, 114(10), E1875-E1884.

21. Stock-Ley, Peter G., N. J. Stonehouse, and K. Valegård. "Molecular mechanism of RNA phage morphogenesis." *International journal of biochemistry* 26.10-11 (1994): 1249-1260.
22. Peabody, D. S. (1993). The RNA binding site of bacteriophage MS2 coat protein. *The EMBO journal*, 12(2), 595-600.
23. Bertrand, E., Chartrand, P., Schaefer, M., Shenoy, S. M., Singer, R. H., & Long, R. M. (1998). Localization of ASH1 mRNA particles in living yeast. *Molecular cell*, 2(4), 437-445.
24. Lionnet, T., Czaplinski, K., Darzacq, X., Shav-Tal, Y., Wells, A. L., Chao, J. A., ... & Singer, R. H. (2011). A transgenic mouse for in vivo detection of endogenous labeled mRNA. *Nature methods*, 8(2), 165.
25. Park, H. Y., Lim, H., Yoon, Y. J., Follenzi, A., Nwokafor, C., Lopez-Jones, M., ... & Singer, R. H. (2014). Visualization of dynamics of single endogenous mRNA labeled in live mouse. *Science*, 343(6169), 422-424.
26. Chao, J. A., Patskovsky, Y., Almo, S. C., & Singer, R. H. (2008). Structural basis for the coevolution of a viral RNA–protein complex. *Nature structural & molecular biology*, 15(1), 103-105.
27. Wu, B., Miskolci, V., Sato, H., Tutucci, E., Kenworthy, C. A., Donnelly, S. K., ... & Hodgson, L. (2015). Synonymous modification results in high-fidelity gene expression of repetitive protein and nucleotide sequences. *Genes & development*, 29(8), 876-886.
28. Harrison, R. G. (1906). Observations on the living developing nerve

fiber. Proceedings of the society for experimental biology and medicine, 4(1), 140-143.

- 29. Moon, H. C., & Park, H. Y. (2016). Imaging Single mRNA Dynamics in Live Neurons and Brains. In Methods in enzymology (Vol. 572, pp. 51-64). Academic Press.**

2. Generation of Arc-PBS mouse

2.1 Introduction

As Arc gene is appreciated as a key molecule for understanding mechanism of memory formation, several transgenic Arc mouse models have been generated. Arc KO mouse which entire Arc gene is deleted was viable whereas KO mouse from another experiment with remaining neomycin cassette and partially deleted coding sequence died during embryogenesis [1, 2]. Viable Arc KO mouse with whole Arc gene deletion exhibited impaired long-term memory while short-term memory was intact. Also, whereas early phase long term potentiation (LTP) was unimpaired, late phase LTP was impaired. Especially, long term depression (LTD) was effectively reduced [2]. Approaches utilizing tamoxifen (TM) - dependent Cre recombinase (CreERT2) were possible to permanently mark the population of neurons which Arc has been transcribed in time window ranging up to 12 hours after the injection of

TM. This permanent marking of Arc transcribed cells enabled comparing two populations of cells with Arc transcription after two distinct events from the same mouse [3, 4]. However, depending on experimental purpose, time window of 12 hours might be too long. And the caveat is CreERT2 which was expressed before the stimulus, however not yet degraded and present at cytoplasm, can also be activated by TM. Dr. Tonegawa's group substituted Arc protein with enhanced green fluorescent protein (eGFP) protein to perform live mouse imaging which enables continuous tracking of Arc promoter activity from same population of neurons. This substitution is essentially knock-out of Arc gene from allele. By comparing homozygous, heterozygous and wild-type mice, authors revealed Arc's role in sculpting orientation specificity in visual cortex [5]. However, due to the time needed for maturation of fluorescent chromophore, there must be some delay between actual onset of promoter activity and eGFP signal. Finally, there was a transgenic mouse line which expresses extra linearized Arc promoter-mGFP-Arc transgene. Using this transgenic mouse, Dr. Bito's group showed CamkII β dependent synaptic accumulation of Arc *in vivo* [6]. Later, this mGFP-Arc transgene line was investigated again to test the effect of RNA splicing on Arc mRNA dendritic transport and nonsense mediated decay (NMD) [7]. Due to the lack of splicing of mEGFP-Arc mRNA, NMD was suppressed. Therefore, basal level of Arc mRNA and protein were high. Also, mEGFP-Arc mRNAs didn't enter dendrite efficiently compared to the endogenous Arc mRNAs. Thus, intact splicing

of 3'UTR is important for both dendritic transport and NMD of Arc mRNA. Here, we generated a transgenic mouse which enables observing dynamics of Arc transcription in real time using PP7 system. In this chapter, generation and validation process of Arc-PBS transgenic mouse will be described.

2.2 Materials and Methods

Generation of Arc-PBS knock-in mouse

Animal care and experimental procedures were carried out in accordance with the protocols approved by the Institutional Animal Care and Use Committee (IACUC) at Albert Einstein College of Medicine, Janelia research campus of Howard Hughes Medical Institute, and Seoul National University. Targeting construct for Arc allele was produced by using conventional cloning approaches with homology arms amplified from C57BL/6J mouse BAC vector RPCI-23-81J22. After verification by sequencing, the targeting construct was electroporated into 129S6 × C57BL/6 F1 hybrid embryonic stem (ES) cell line. ES cell clones were screened for homologous recombination by PCR. Correctly targeted ES cells were microinjected into BL/6 blastocysts, and chimeras were mated to FLP_eR mice (ROSA26::FLP) to remove the FRT-flanked neomycin resistance cassette in the offspring. Pups without the PGK-neo cassette were identified by PCR and used to backcross to a C57BL/6J background. Experiments were performed using either non-backcrossed mouse line

or 7th backcross generation line. We have not observed any qualitative difference between non-backcross and 7th backcross generation mice.

Genotyping

For genotyping of Arc-PBS knock-in mice, we performed PCR reactions using the following primer sets. For the 5' end, we used two forward primers, Arc PBS gt 5F (5'-TGTCCAGCCAGACATCTACT-3') and ArcPBS gt 5R (5'-TAGCATCTGCCCTAGGATGT-3'), and one reverse primer PBS scr R1 (5'-GTTTCTAGAGTCGACCTGCA -3'), yielding 320-bp product for the WT allele and 228-bp product for the PBS knock-in allele. For the 3' end, we used a forward primer Arc PBS gt 3F (5'-GACCCATACTCATTTGGCTG-3') and a reverse primer ArcPBS gt 3R (5'-GCCGAGGATTCTAGACTTAG-3'), yielding 332-bp product for the WT allele and 413-bp product for the PBS knock-in allele. PCR conditions were 94° C 30 sec, 55° C 30 sec, 72° C 30 sec for 35 cycles.

Hippocampal neuron culture

Hippocampi were dissected out from postnatal day 1(P1) pups from Arc^{P/+} heterozygous x heterozygous mice. Hippocampal neurons were isolated as described before [9]. Dissected hippocampi were kept at ice cold neural dissection

solution (NDS) (10 mM Hank's balanced salt solution (HBSS) (Gibco, cat No. 14185) and 19 mM HEPES (Gibco, cat. No. 15630-080) in water). After collection, hippocampi were digested with 0.25% Trypsin in NDS at 37° C for 15 mins, followed by trituration. After trituration, trypsin was removed and media was changed to plating medium (PM) (10% FBS heat inactivated (Gibco, cat. No. 10082-147), 1x Glutamax (Gibco, cat. No. 35050-061) and 0.1 mg/ml Primocin (Invivogen, cat. No. ant-pm-1) in Neurobasal A medium (Gibco, cat. No. 10888-022)). Hemocytometer was used to count the density of hippocampal neurons. Hippocampal neurons were plated onto overnight PDL-coated Mattek dishes with the appropriate density (200 µl of 425,000 cells/ml). After 4 hours incubation in the 37° C, 5% CO₂ incubator, 1.8 ml of equilibrated B27 medium (1x B27 (Gibco, cat. No. 17504-044), 1x Glutamax (Gibco, cat. No. 35050-061) and 0.1 mg/ml primocin (Invivogen, cat. No. ant-pm-1) in Neurobasal A medium (Gibco, cat. No. 10888-022)) was added to each dish. Every 7 days after seeding, gently add 300 µl of equilibrated B27 medium to the cells. Because neurons are too vulnerable, it is recommended to refrain from taking neurons out of incubator.

Western blot

Brain tissue extracts were prepared using T-PER tissue protein extraction reagent (Thermo scientific) containing 1× protease inhibitor (Roche). Three 5-week-old

female wild-type and Arc-PBS mice were sacrificed according to IACUC guidelines. 32 μ g of protein was separated on 4-12% Bis-Tris polyacrylamide precast gels in MES-SDS running buffer and transferred to nitrocellulose membranes by using the Mini Blot Module following the manufacturer's instructions (Thermo scientific). The following antibodies were used: anti-Arc (1:200, sc-17839, Santa Cruz Biotechnology) and anti-GAPDH (1:100,000, G9545, Sigma) as primary antibodies, and anti-rabbit IgG conjugated to HRP (1:5,000, SA002, GenDEPOT), and anti-mouse IgG conjugated to HRP (1:5,000, SA001, GenDEPOT) as secondary antibodies. Pierce ECL western blotting substrate (Thermo scientific) was used for HRP detection. Western blots were imaged by LAS 4000 (GE Healthcare Life Sciences). The images were analyzed by Image Studio Lite Ver 5.2 (LI-COR Biosciences).

smFISH

DIV 15 neurons were stimulated with 50 μ M bicuculline and fixed with 4% paraformaldehyde (PFA) in phosphate-buffered saline (PBS). After permeabilization with 0.1% Triton X-100 in PBS for 10 min at room temperature (RT), the cells were prehybridized with 10% formamide in 2 \times SSC for 30 min at RT. Hybridization was performed at 37°C for 3 h using hybridization buffer (~10 ng of 20-mer DNA probes, 2 \times SSC, 10% formamide, 10% dextran sulfate, 2 mg/ml

bovine serum albumin (BSA), 0.025 mg/ml *Escherichia coli* transfer RNA, and 0.025 mg/ml sheared salmon sperm DNA in ribonuclease (RNase)-free water). The cells were then washed twice with warm 10% formamide in 2× SSC for 20 min, followed by multiple washings with 2× SSC and DAPI staining.

Image analysis

Single mRNAs and transcription sites were detected using AIRLOCALIZE [8]. The number of nascent mRNAs were calculated by dividing detected intensity of transcription sites by single mRNA intensity from the same neuron in both channels.

Probe Name/No.	Sequence (20nt)	Dye
Arc CDS_1	cgtgaccaaggtctaagaga	Quasar 670
Arc CDS_2	attgccgctgtacacaagtc	Quasar 670
Arc CDS_3	tggagatcttggtggaaggc	Quasar 670
Arc CDS_4	ttcaggaactgcgcacaa	Quasar 670
Arc CDS_5	ctagctctcaatcaacagg	Quasar 670
Arc CDS_6	gcttcaaacagcttcatgtc	Quasar 670
Arc CDS_7	atgataagccaggccaacaa	Quasar 670
Arc CDS_8	gcagcaaggatactggacac	Quasar 670
Arc CDS_9	acctagatcatgttcagac	Quasar 670
Arc CDS_10	cctggacttagtgaagatgg	Quasar 670

Arc CDS_11	gcggaaaagcctttcaactg	Quasar 670
Arc CDS_12	ctgggtctttgtggaagatg	Quasar 670
Arc CDS_13	aggtatctgcgtttcttctt	Quasar 670
Arc CDS_14	tagatgctggtggttagg	Quasar 670
Arc CDS_15	gagggccaatcaggaagaag	Quasar 670
Arc CDS_16	aagcgggagtagaaactggc	Quasar 670
Arc CDS_17	gcacatagaaggagagta	Quasar 670
Arc CDS_18	aaggtccacattgcagtg	Quasar 670
Arc CDS_19	aagagtggtgctcaactg	Quasar 670
Arc CDS_20	aaagcttcacctgtagtg	Quasar 670
Arc CDS_21	attgatggaggtatgcatcc	Quasar 670
Arc CDS_22	gggtgaggatgactgtcaat	Quasar 670
Arc CDS_23	ctgaggaaagccagcaggac	Quasar 670
Arc CDS_24	atggccataggattgctgac	Quasar 670
Arc CDS_25	tccaccaagtctgaagcag	Quasar 670
Arc CDS_26	gaactccttacattccatcc	Quasar 670
Arc CDS_27	atgggtagagtagctgttg	Quasar 670
Arc CDS_28	atgctgctcagttaggaac	Quasar 670
Arc CDS_29	gctcttgagtacataactcc	Quasar 670
Arc CDS_30	tgcagatgtgaccttaacc	Quasar 670
Arc CDS_31	ggctgtagaagccagtata	Quasar 670
Arc CDS_32	caataccagtgtagcagag	Quasar 670
Arc CDS_33	gcatattcagcacaactgtt	Quasar 670
Arc CDS_34	acagaatggccacacttgag	Quasar 670

Arc CDS_35	caaaactctgccttgagct	Quasar 670
Arc CDS_36	ccctaacactttggggagag	Quasar 670
Arc CDS_37	ctttaaagatctgtagccca	Quasar 670
Arc CDS_38	cagcctaaagcttctgagac	Quasar 670
Arc CDS_39	tagcatttctgctgggattg	Quasar 670
Arc CDS_40	ctcagctcctacaggagatg	Quasar 670
Arc CDS_41	ttatccaggaggcttctactg	Quasar 670
Arc CDS_42	tagcagacacgtgacttagc	Quasar 670
Arc CDS_43	catcgcgttgaaagcgacac	Quasar 670
Arc CDS_44	ctaggcctcctttttattt	Quasar 670
Arc CDS_45	tggggtcatacgcataaagc	Quasar 670
Arc CDS_46	aaaacagtttagcccagagg	Quasar 670
Arc CDS_47	aagcaaaggccttctcag	Quasar 670
Arc CDS_48	gtagcttcaagggatcttc	Quasar 670
LK 20	tttctagagtcgacctgcag	Quasar 570
LK 51-1	ctaggcaattaggtaccttag	Quasar 570
LK 51-2	ctaataaccgggaataactg	Quasar 570

Table 1. Sequence of the probes used for smFISH against the Arc coding sequence (CDS) and linker sequence (LK). Arc CDS Probe sets are modified at 3'ends for conjugation to Quasar 670. LK probes sets are modified at both 5' and 3'ends. CDS probes are labeled with Quasar 670 (Biosearch) and LK probes are labeled with Quasar 570 (Biosearch).

2.3 Results and Discussion

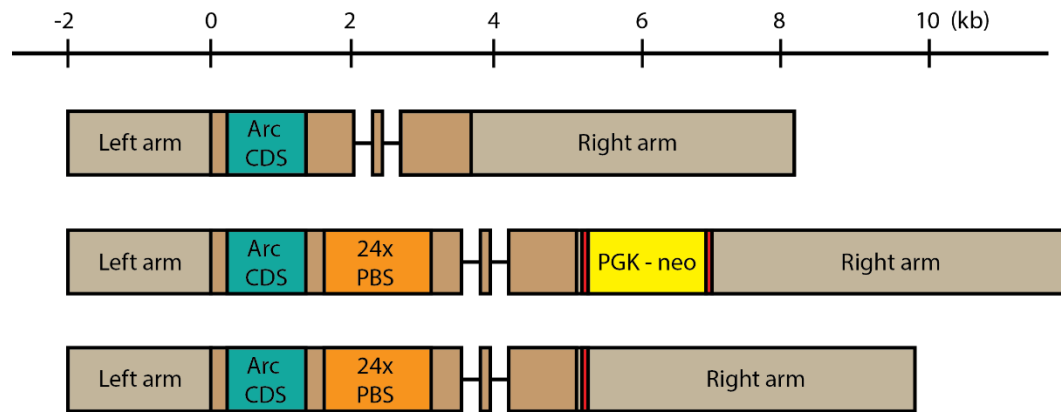


Figure 2.1 Schematics of the endogenous Arc locus, Arc-PBS targeting construct, and the final targeted locus.

The Arc gene consists of three exons spanning 3.5 kilo–base pairs (kbp) and encodes for the 396–amino acid Arc protein. To label full-length Arc mRNA, we inserted a 1.5-kbp cassette containing 24 repeats of the PBS stem-loop motif in the 3'UTR of the Arc gene (Figure 2.1). To avoid disruption of evolutionarily conserved cis-acting regulatory elements, we aligned the sequences of the Arc genes in chicken, mouse, rat, and human and 250 nucleotides after the stop codon was targeted for insertion in a non-conserved region. The knock-in of the PBS cassette was performed by homologous recombination, and the embryonic stem (ES) colonies were selected on the basis of neomycin resistance and polymerase chain reaction (PCR). ES cell clones screened for homologous recombination were microinjected into blastocysts, and chimeras were mated to FLPeR mice

(ROSA26::FLP) to remove the FLP recombinase target (FRT)-flanked neomycin resistance cassette. Arc-PBS mouse pups without the neomycin cassette were used to backcross to a C57BL/6 background. Experiments were performed on 7th or higher backcross generation mice.

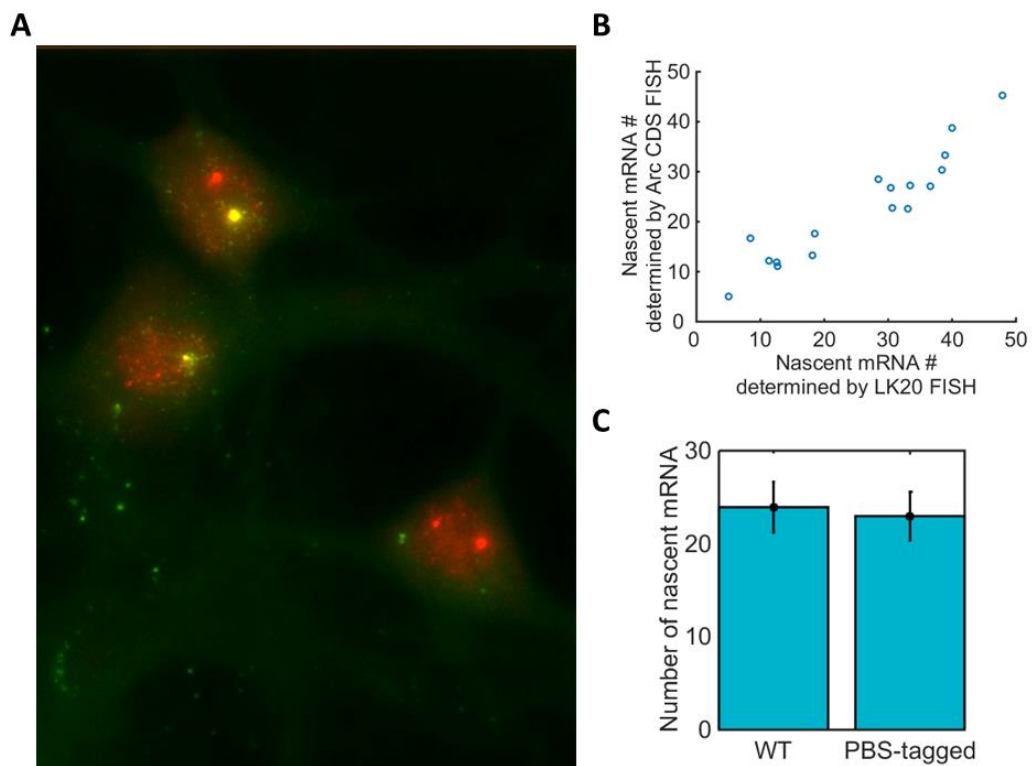


Figure 2.2 Arc transcriptional output is not altered by PP7 knock-in.

(A) Representative image of neurons with Arc transcription sites from Arc-PBS KI heterozygous x heterozygous cultured neurons. PBS-LK Quasar570 (Green) and Arc-CDS Quasar670 probe (Red). Yellow transcription sites are from PBS knocked in alleles whereas red transcription sites are from wildtype alleles. **(B)**

Scatter plot of nascent mRNA numbers of Arc-PBS knocked-in transcription sites by LK 20 mer FISH versus Arc CDS FISH. (n= 17). PBS stem-loop signal reliably recapitulates Arc transcription activity. (C) Average nascent mRNA numbers of untagged allele and tagged allele determined by Arc CDS FISH. Error bars represent standard deviation. (n=18 for untagged alleles, n=17 for tagged alleles.)

To check whether knock-in of PBS repeats doesn't interfere with normal Arc transcriptional activity, we performed single molecule FISH (smFISH) on het x het neuron culture from Arc-PBS mouse. Two sets of FISH probes (Arc CDS and LK 20) which targets Arc coding sequence and linker sequences between PBS stem-loops respectively were used. Offsprings of het x het cultures have genotypes of wildtype, heterozygous, and homozygous. As expected, we could observe all three type of alleles (Figure 2.2A). Nascent mRNA number on transcription site was determined by both Arc CDS probes and LK 20 probes. The Pearson correlation coefficient between nascent mRNA numbers on PBS knocked in transcription sites determined by Arc CDS probes and LK 20 probes was 0.94 suggesting that knocked in PBS stem-loops faithfully visualize Arc transcription activity. However, the slope of linear fitted curve was 1.13 which is larger than 1 (Figure 2.2B). This is expected result because Arc CDS sequence always proceeds PBS sequence during elongation and therefore some portion of mRNAs that

didn't transcribe PBS repeat part will be present. However, the average number of nascent transcripts on transcription sites was not altered by knock-in of PBS stem-loops ($p = 0.8$) (Figure 2.2C).

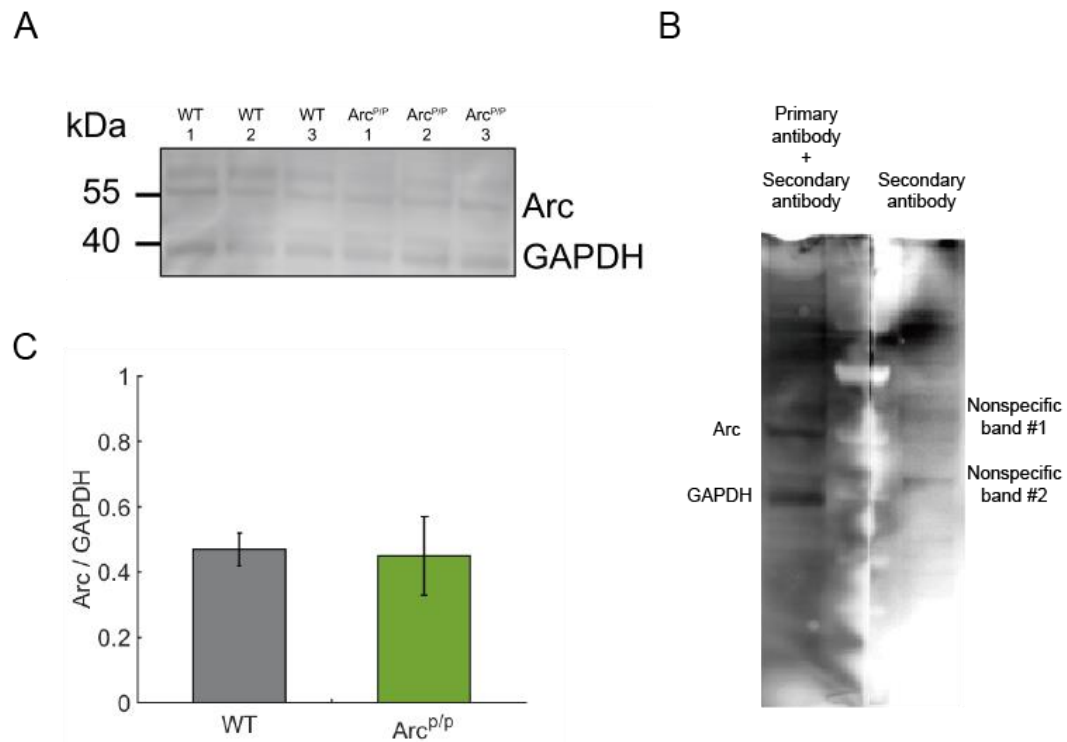


Figure 2.3 Comparison of homozygous Arc-PBS mouse to WT mouse.

(A) Western blot image of Arc protein (55 kDa) and GAPDH protein (36 kDa) in brain tissue lysates from three WT and three homozygous Arc-PBS (Arc^{P/P}) knock-in mice. **(B)** Two nonspecific bands were produced by nonspecific binding of secondary antibody. **(C)** Relative Arc expression quantified using GAPDH as loading control was compared between WT and Arc^{P/P} mice (lower panel). No significant difference was observed ($P > 0.05$, $n = 3$ mice). Error bars represent

standard deviation (SD).

Next, we evaluated the protein level between wildtype and Arc-PBS homozygous mouse in the whole brain level. For statistical analysis, three mice from each genotype were sacrificed in the home cage. Housekeeping gene GAPDH was used as loading control. The nonspecific bands were found out to be originated from nonspecific bindings from secondary antibodies (Figure 2.3A, B). There were no distinguishable differences in the expression levels of Arc protein in wild-type ($Arc^{+/+}$) and homozygous ($Arc^{P/P}$) mice ($p > 0.05$) (Figure 2.3C). Therefore, we showed that Arc expression level of Arc-PBS mouse is not altered in both transcriptional and translational level.

2.4 References

1. Liu, D., Bei, D., Parmar, H., & Matus, A. (2000). Activity-regulated, cytoskeleton-associated protein (Arc) is essential for visceral endoderm organization during early embryogenesis. *Mechanisms of development*, 92(2), 207-215.
2. Plath, N., Ohana, O., Dammermann, B., Errington, M. L., Schmitz, D., Gross, C., ... & Kobalz, U. (2006). Arc/Arg3.1 is essential for the consolidation of synaptic plasticity and memories. *Neuron*, 52(3), 437-444.
3. Denny, C. A., Kheirbek, M. A., Alba, E. L., Tanaka, K. F., Brachman, R. A., Laughman, K. B., ... & Hen, R. (2014). Hippocampal memory traces are differentially modulated by experience, time, and adult neurogenesis. *Neuron*, 83(1), 189-201.
4. Guenther, C. J., Miyamichi, K., Yang, H. H., Heller, H. C., & Luo, L. (2013). Permanent genetic access to transiently active neurons via TRAP: targeted recombination in active populations. *Neuron*, 78(5), 773-784.
5. Wang, K. H., Majewska, A., Schummers, J., Farley, B., Hu, C., Sur, M., & Tonegawa, S. (2006). In vivo two-photon imaging reveals a role of arc in enhancing orientation specificity in visual cortex. *Cell*, 126(2), 389-402.
6. Okuno, H., Akashi, K., Ishii, Y., Yagishita-Kyo, N., Suzuki, K., Nonaka, M., ... & Natsume, R. (2012). Inverse synaptic tagging of inactive synapses via dynamic interaction of Arc/Arg3.1 with CaMKII β . *Cell*, 149(4), 886-898.

- 7. Steward, O., Matsudaira Yee, K., Farris, S., Pirbhoy, P. S., Worley, P., Okamura, K., ... & Bito, H. (2018). Delayed degradation and impaired dendritic delivery of intron-lacking EGFP-Arc/Arg3. 1 mRNA in EGFP-Arc transgenic mice. *Frontiers in molecular neuroscience*, 10, 435.**
- 8. Lionnet, T., Czaplinski, K., Darzacq, X., Shav-Tal, Y., Wells, A. L., Chao, J. A., ... & Singer, R. H. (2011). A transgenic mouse for in vivo detection of endogenous labeled mRNA. *Nature methods*, 8(2), 165.**
- 9. Moon, H. C., & Park, H. Y. (2016). Imaging Single mRNA Dynamics in Live Neurons and Brains. In *Methods in enzymology* (Vol. 572, pp. 51-64). Academic Press.**

3. Ca²⁺ activity and Arc transcription

3.1 Introduction

Immediate early genes (IEGs) are genes that are rapidly and transiently induced by diverse cellular stimuli [1]. Arc is an IEG that is responsive to neural activity. Within 5 min after exploration to novel environment, percentage of neurons with Arc transcription ON increased to 45 % in rat hippocampal CA1 region. This is very large increase compared to ~5% of activation rate in home caged rat [2]. However, as some time is needed for anesthesia, decapitation and complete freezing of the brain, actual time point of Arc transcription snapshot observed might be longer than 5 min after the start of the exploration. Also in this pioneering study, maximum electroconvulsive shock (MECS) was given to rat. Precisely time controlled MECS or seizure could induce Arc transcription within 5 min. Since then, this causality between neural activity and Arc transcription has been widely used as

a rationale for considering neurons with Arc transcription site same as the neurons that underwent high neural activity within 5 min.

How does Arc transcription initiate in response to neural activity? There must be some kind of molecule that senses neural activity. Signal transduction inside cell can happen mainly in two ways. First pathway is kinase and phosphatase involving signal transduction. Kinase phosphorylates protein and phosphatase de-phosphorylates target. And these phosphorylation or de-phosphorylation event can change the structure of target protein thus changing the activation status of the target. Cascades of these phosphoryl group addition or deletion events transduce signal to different cellular compartments. In postsynaptic compartment, there exist two classes of glutamatergic receptors. First group is ionotropic receptor (iGluR) and second group is metabotropic receptor (mGluR). Metabotropic receptor is member of G-protein coupled receptors (GPCRs). After binding of glutamate, mGluR activates G protein and the following signal cascades happen. However, this process can be slow compared to ionotropic receptor dependent signal transduction especially in case of synapse to nucleus signal transduction in neurons [3-5]. The other mechanism of signal transduction is by change in concentration of second messengers such as Ca^{2+} . Basal intracellular Ca^{2+} levels are usually kept low by ion pumps. This is because Ca^{2+} functions as second messenger in diverse processes thus keeping basal Ca^{2+} level low can maximize the dynamic range of Ca^{2+} signaling. Once glutamate binds to ionotropic glutamatergic receptor, ion channel

opens and this opening triggers new equilibrium of ion concentrations. Especially, Ca^{2+} input from NMDA receptor is important for proper functioning of synaptic plasticity. This is because multiple kinases are activated by high concentration of Ca^{2+} ion. For example, increased concentration of Ca^{2+} promotes calmodulin (CaM) binding to Ca^{2+} and thus activating Ca^{2+} /calmodulin-dependent protein kinases (CaMKs). This Ca^{2+} mediated signal transduction is believed to be better for fast induction of Arc transcription compared to metabotropic induction. This is because Ca^{2+} concentration can dramatically change inside the nucleus which is the place where the transcription actually happens. In 2001, Hilmar Bading's group showed that nuclear Ca^{2+} spikes can induce cAMP response element-binding protein (CREB) mediated gene expression [6]. They used wheat germ agglutinin (WGA) which blocks nuclear import of any protein. Even after blocking nuclear import of proteins, they could observe CREB mediated transcription.

Based on these powerful observations, somatic Ca^{2+} activity and neural IEG transcription seems to be in the relationship of one-to-one correspondence [7-9]. However, due to lack of ability to image transcription in real time, it was impossible to simultaneously image both Ca^{2+} activity and transcription activity from the same neuron. Only the correlations were shown by indirect analogy. Here, with this new Arc-PBS mouse and live cell imaging, we reveal some disparity between relationship of Ca^{2+} activity and Arc transcription activity in neuron culture.

3.2 Materials and Methods

Hippocampal neuron culture

Hippocampi were dissected out from postnatal day 1(P1) pups from Arc^{P/P} homozygous mice. Hippocampal neurons were isolated as described before [9]. Dissected hippocampi were kept at ice cold neural dissection solution (NDS) (10 mM Hank's balanced salt solution (HBSS) (Gibco, cat No. 14185) and 19 mM HEPES (Gibco, cat. No. 15630-080) in water). After collection, hippocampi were digested with 0.25% Trypsin in NDS at 37° C for 15 mins, followed by trituration. After trituration, trypsin was removed and media was changed to plating medium (PM) (10% FBS heat inactivated (Gibco, cat. No. 10082-147), 1x Glutamax (Gibco, cat. No. 35050-061) and 0.1 mg/ml Primocin (Invivogen, cat. No. ant-pm-1) in Neurobasal A medium (Gibco, cat. No. 10888-022)). Hemocytometer was used to count the density of hippocampal neurons. Hippocampal neurons were plated onto overnight PDL-coated Mattek dishes with the appropriate density (200 µl of 425,000 cells/ml). After 4 hours incubation in the 37° C, 5% CO₂ incubator, 1.8 ml of equilibrated B27 medium (1x B27 (Gibco, cat. No. 17504-044), 1x Glutamax (Gibco, cat. No. 35050-061) and 0.1 mg/ml primocin (Invivogen, cat. No. ant-pm-1) in Neurobasal A medium (Gibco, cat. No. 10888-022)) was added to each dish. Every 7 days after seeding, gently add 300 µl of equilibrated B27 medium to the cells. Because neurons are too vulnerable, it is recommended to refrain from taking neurons out of incubator.

Preparation of viruses

Coding sequences for NLS-stdPCP-stdGFP were cloned into AAV expression vectors. The synonymous versions of PCP (stdPCP) and GFP (stdGFP) were designed based on previously described coat proteins and fluorescent proteins (32). Serotype 2/1 AAV vector for expression of hSyn-NLS-stdPCP-stdGFP was generated using the AAV Helper-Free System (Agilent Technologies). The final concentration of AAV infection was $\sim 10^9$ genome copies per ml (GC/ml). After infection with AAV, no media change was performed.

Two-color imaging of calcium and Arc transcriptional dynamics

Neurons were infected with AAV-hSyn-NLS-tdPCP-tdGFP on DIV 6-7. Live-cell imaging experiments were performed on DIV 14-17. 2 μ l of 2 mM Red-shifted Ca^{2+} indicator (Ca^{2+} Orange, Molecular probes) was added to neurons in 2 ml of NGM and neurons were incubated in 37°C, 5% CO_2 incubator for 30 mins. Then cells were washed twice with warm HEPES-buffered saline (HBS; 119 mM NaCl, 5 mM KCl, 2 mM CaCl_2 , 2 mM MgCl_2 , 30 mM D-glucose, 20 mM HEPES in DI water at pH 7.4) and placed in 37°C, 5% CO_2 incubator for 30 mins again.

After 30 mins of incubation, neurons were imaged by using a wide-field fluorescence microscope equipped with Ixon ultra DU-897U EMCCD camera (Andor), UApo 150 \times oil immersion objective (Olympus), MS-2000-500 XYZ

automated stage (ASI) and IX73 microscope body (Olympus). CU-201 heating chamber (Live Cell Instrument) was used to maintain the temperature at 37°C. The Micro-Manager software was used for image acquisition. Fluorescence excitation source was SOLA SE white LED (Lumencor) and appropriate filter sets were used for fluorescence observation (49002 ET-EGFP filter set (Chroma) for GFP-tagged Arc mRNA observation and 49004 ET-Cy3/TRITC filter set (Chroma) for Ca²⁺ activity observation). First, a z-section image of a neuron was taken in green fluorescence channel to visualize basal Arc mRNA transcription. Then, time-lapse images of baseline Ca²⁺ activity was acquired for 4-6 min with 500 ms exposure time in red fluorescence channel. After 50 µM bicuculline was added, induced Ca²⁺ activity was imaged for 4-5 min followed by z-section images of Arc mRNA transcription every 2 min starting from 5 min until 27 min. Finally, Ca²⁺ activity was imaged again for 4-7 min.

smFISH-IF

For simultaneous detection of phosphorylated CREB and Arc transcription, combination of smFISH and immunofluorescence (smFISH-IF) was performed. AAV viral infection (AAV-hSyn-NLS-tdPCP-tdGFP) was done on DIV 6-7. After being placed in 37°C, 5% CO₂ incubator for 20 min with 50 µM bicuculline, neurons were fixed for 20 min with cold 4% PFA, 4% sucrose in PBS-MC.

Quenching was done for 15 min with 50 mM glycine in PBS-MC. Neurons were permeabilized for 15 min with cold 0.1% Triton X-100 and 0.5% BSA in PBS-MC. Blocking and pre-hybridization was performed for 30 min at room temperature (RT) with 10% formamide, 2x SSC, and 0.5% BSA in RNase-free water. Hybridization of FISH probes and primary antibody were done together. Neurons were incubated in 37°C for 3 hours with 10 ng of Arc CDS probes and primary antibody against Ser133 residue phosphorylated CREB (06-519, Millipore) in hybridization buffer. Neurons were quickly washed twice with warm 10% formamide, 3% BSA in 2x SSC. Then, hybridization with secondary antibody were performed twice with Alexa Fluor 647 conjugated secondary antibody (A21245, Thermofisher) in 10% formamide and 2x SSC in RNase-free water at 37°C for 20 min each. After washing 4 times with 2x SSC, nuclei were stained with DAPI [10].

Image analysis

For analyzing the data from simultaneous imaging of Arc transcription and Ca²⁺ activity, time-lapse Arc transcription activity plot was generated by using custom-made transcription analysis program utilizing a part of u-track [11], which detected transcription sites and calculated the intensity amplitude from 2D Gaussian fitting. Ca²⁺ plots were obtained by using FluoroSNNAP program [12] and custom-made MATLAB program which calculates $\Delta F/F$ of the region of interest. $\Delta F/F$ was

calculated by three steps. First, rolling average of 4 frames was done to reduce the noise. Next, the average fluorescence (F) was subtracted by the baseline fluorescence (F₀) which was the mean of fluorescence from the lowest 6 frames (10%) among the previous 60 frames. Finally, $\Delta F/F \equiv (F-F_0)/F_0$ was calculated. The average fluorescence intensities of pCREB in the nucleus and background were obtained using ImageJ [13]. The background-subtracted value of pCREB intensity was considered as pCREB level in the nucleus.

Probe Name/No.	Sequence (20nt)	Dye
Arc CDS-1	ttaccaatctgcaggatcac	Quasar 570
Arc CDS-2	ttggacacttcggtaacag	Quasar 570
Arc CDS-3	caagttgtctccagcttgc	Quasar 570
Arc CDS-4	caaagacaggccttgatgga	Quasar 570
Arc CDS-5	acgtgcatctcacgcttgac	Quasar 570
Arc CDS-6	ctctccagacggtagaagac	Quasar 570
Arc CDS-7	acacctacagagacagtgtg	Quasar 570
Arc CDS-8	tgatggcataggggctaacg	Quasar 570
Arc CDS-9	cccaagactgatattgctga	Quasar 570
Arc CDS-10	ctcgaagatctgtgatcca	Quasar 570
Arc CDS-11	cagccaatattcttcagagc	Quasar 570
Arc CDS-12	tgaactcccaccacttcttg	Quasar 570

Arc CDS-13	aaactccttcttgaactcca	Quasar 570
Arc CDS-14	tgaatggcttcacgggagag	Quasar 570
Arc CDS-15	cagaggaactggtcgagtgg	Quasar 570
Arc CDS-16	catacagtgtctgttacagg	Quasar 570
Arc CDS-17	catactgaatgatctcctce	Quasar 570
Arc CDS-18	agaaagcgcttgagtttggg	Quasar 570
Arc CDS-19	ctctggataagctgctccag	Quasar 570
Arc CDS-20	ctactgactcgttgtaaga	Quasar 570

Table 1. Sequence of the probes used for smFISH against the Arc coding sequence (CDS). Probe sets are modified at both 5' and 3' ends for conjugation to dye of choice. CDS probes are labeled with Quasar 570 (Biosearch).

3.3 Results and Discussion

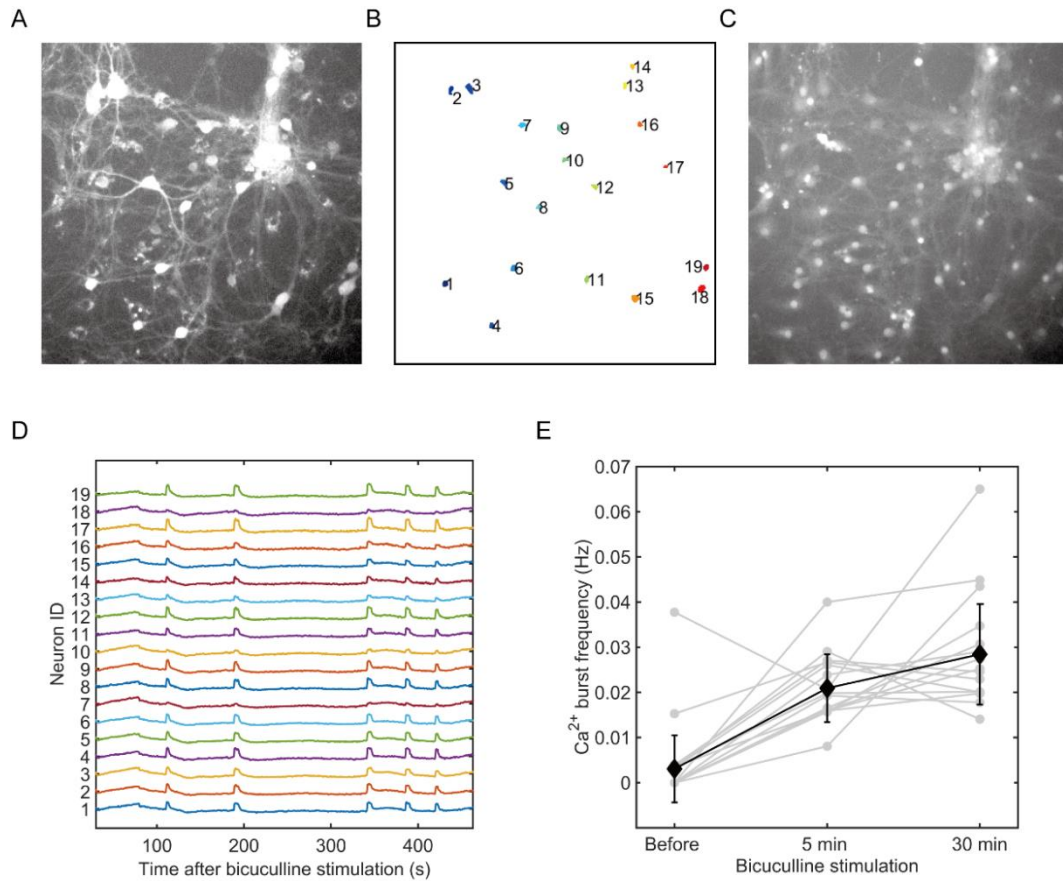


Figure 3.1 Synchronized Ca²⁺ activity during bicuculline incubation. (A) GFP channel image showing AAV-hSyn-NLS-tdPCP-tdGFP infected neurons (DIV 14) imaged using a 20× magnification objective. (B) Somas of GFP positive neurons were selected to be analyzed. (C) Cy3 channel image showing Calcium Orange stained neurons. (D) Synchronized Ca²⁺ activities induced by 50 μM bicuculline incubation. Most of neurons showed synchronized Ca²⁺ spikes. (E) Ca²⁺ burst frequency change during bicuculline stimulation (n = 46 neurons from 2 different

cultures). Error bars represent SD.

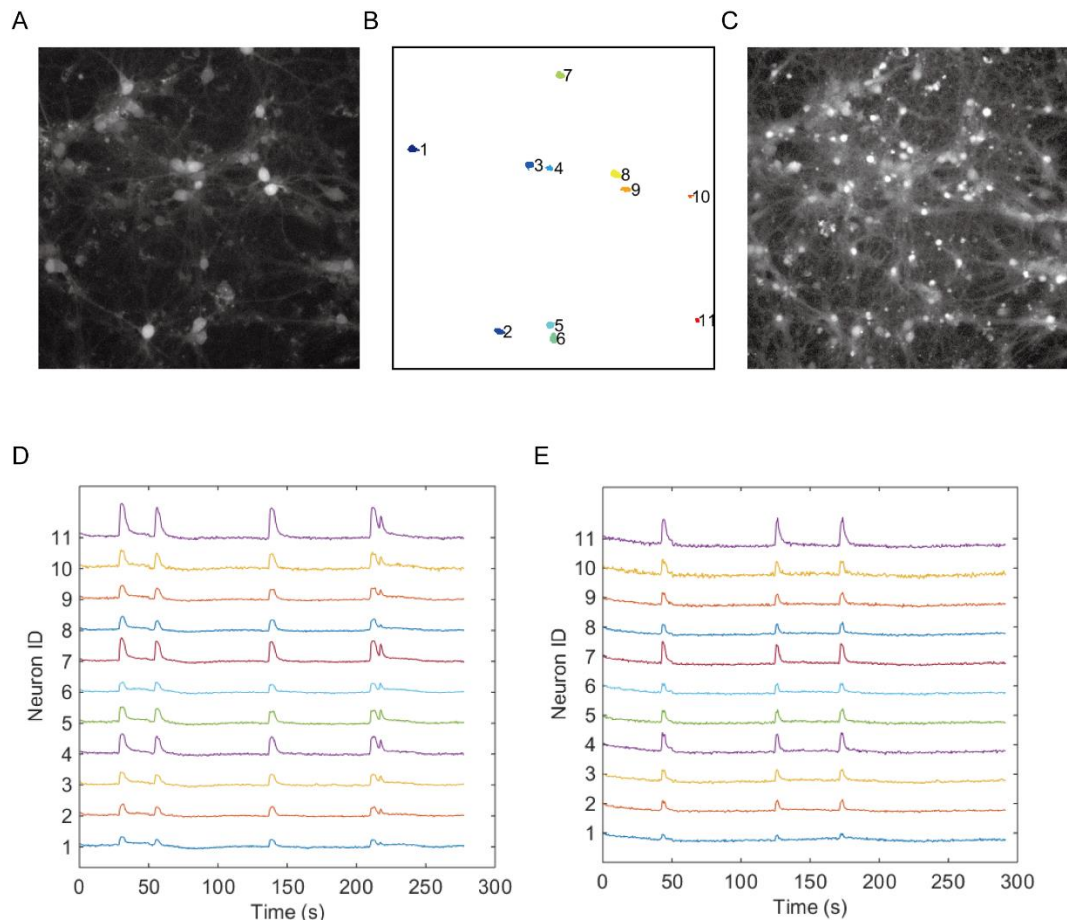


Figure 3.2 Persistent synchronized Ca^{2+} activities after bicuculline washout. (A) GFP channel image showing AAV-hSyn-NLS-tdPCP-tdGFP infected neurons (DIV 10) imaged using a 20 \times magnification objective. **(B)** Somas of GFP positive neurons were selected to be analyzed. **(C)** Cy3 channel image showing Calcium Orange stained neurons. **(D)** Synchronized Ca^{2+} activities 20 min after washout of bicuculline. **(E)** Synchronized Ca^{2+} activities 60 min after washout of bicuculline.

We first characterized the Ca^{2+} dynamics of dissociated hippocampal neuron culture. As bicuculline is an antagonist of GABA receptor, bicuculline treatment inhibits inhibitory action of inhibitory neurons. Therefore, bicuculline treatment elicits burst of synchronized neuronal activity in dissociated hippocampal neuron culture or seizure *in vivo*. 5 min after bicuculline treatment, frequency of Ca^{2+} activity which was less than 0.006 Hz in basal condition increased up to 0.02 Hz. And this synchronized Ca^{2+} burst was still present 30 min after bicuculline treatment (Figure 3.1). Next, we checked how long Ca^{2+} bursts persist after washout of bicuculline. Even 60 min after washout of bicuculline, synchronous Ca^{2+} activity still existed (Figure 3.2). This is probably because of highly connected network within dissociated cultured neurons.

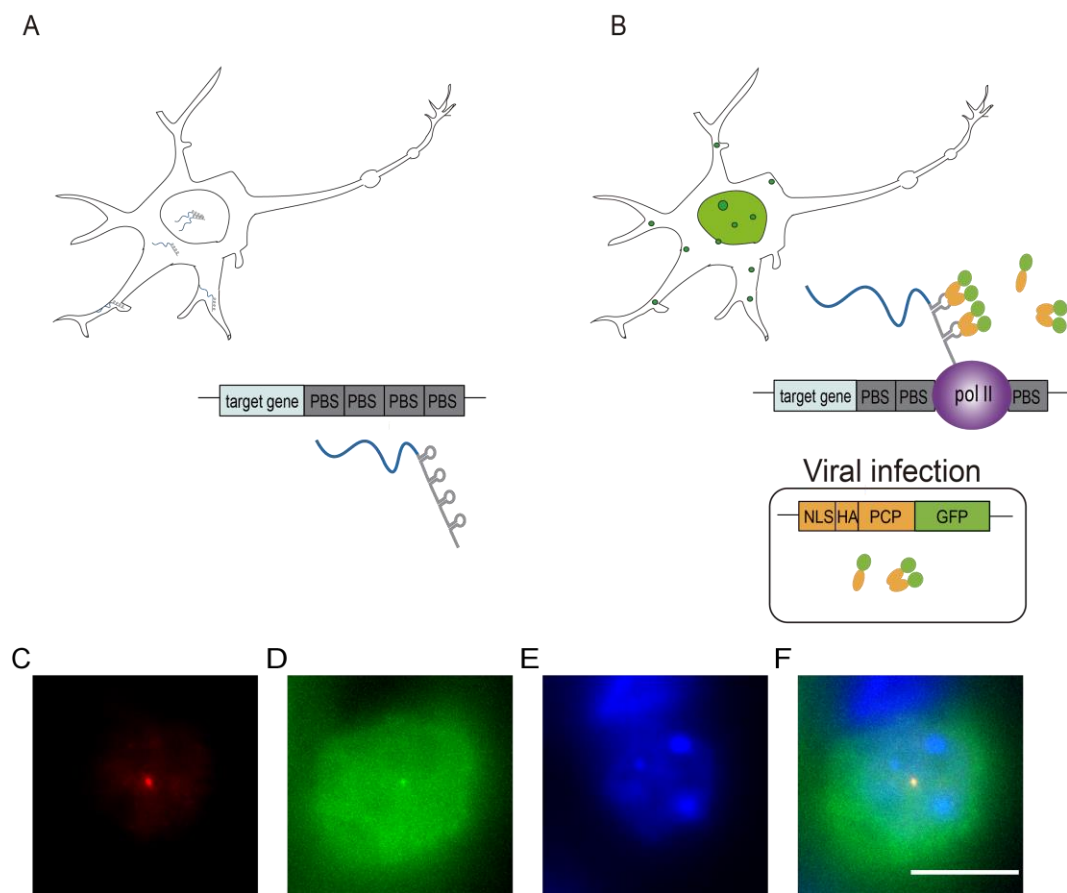


Figure 3.3 Tagging of Arc transcription sites by tdPCP-tdGFP (A) Schematic of Arc DNA and Arc mRNA from Arc-PBS mouse. **(B)** Tagging of endogenous Arc mRNA by exogenous PCP-GFP expression. **(C)** Arc transcription site visualized by linker targeting FISH probes (Q570). **(D)** Arc transcription site visualized by tdPCP-tdGFP tagging. **(E)** DAPI stained nucleus. **(F)** Composite image of 3 channels. FISH (Red), tdPCP-tdGFP (Green), and DAPI (Blue). Scale bar represents 10 μm .

To image Arc transcription activity, we needed to infect AAV for NLS-HA-tdPCP-tdGFP (Figure 3.3). Upon transcription of Arc mRNA, tdPCP-tdGFP binds to PBS stem loops providing enough contrast to observe single Arc mRNA in the cytoplasm. Not only in the cytoplasm but also in the nucleus where some background is present, we can observe Arc mRNA transcription process. That is because Arc mRNA transcription exhibits such a burst-like behavior, dozens of Arc transcripts are densely produced at the gene locus of Arc. Tagging of Arc transcription sites by tdPCP-tdGFP was also verified by smFISH (Figure 3.3).

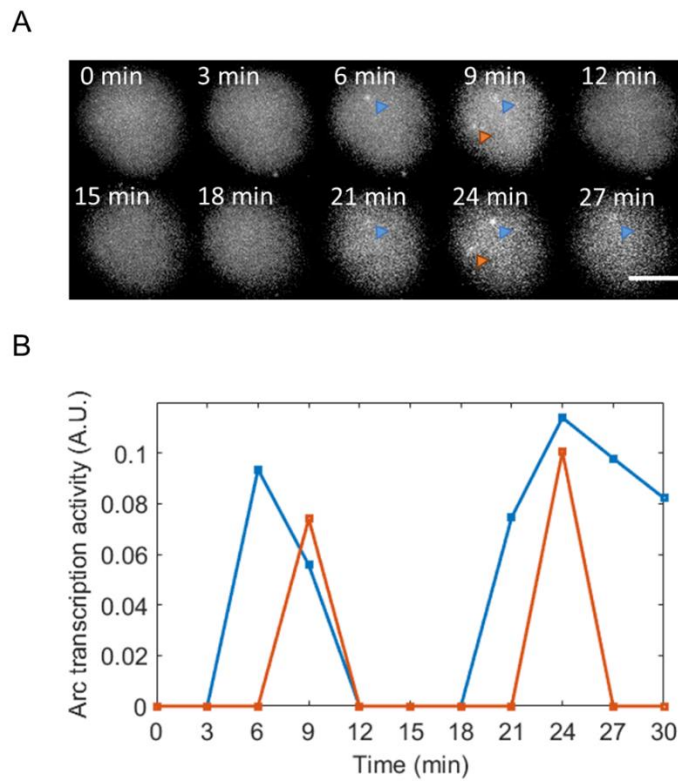


Figure 3.4 Blinking of Arc transcription. (A) Time-lapse images of Arc transcription. Scale bar represents 5 μm . (B) Time-course of Arc transcriptional activity was analyzed by custom matlab program. 2D gaussian fitted amplitude of transcription site was used to describe Arc transcription activity of each allele.

We imaged z-stack image of whole nucleus for 30 min with 3 min intervals. Interestingly, we could observe blinking of Arc transcription sites (Figure 3.4). Thus, snapshot of Arc transcription site from the previous studies might have missed some part of Arc promoter dynamics in short timescale.

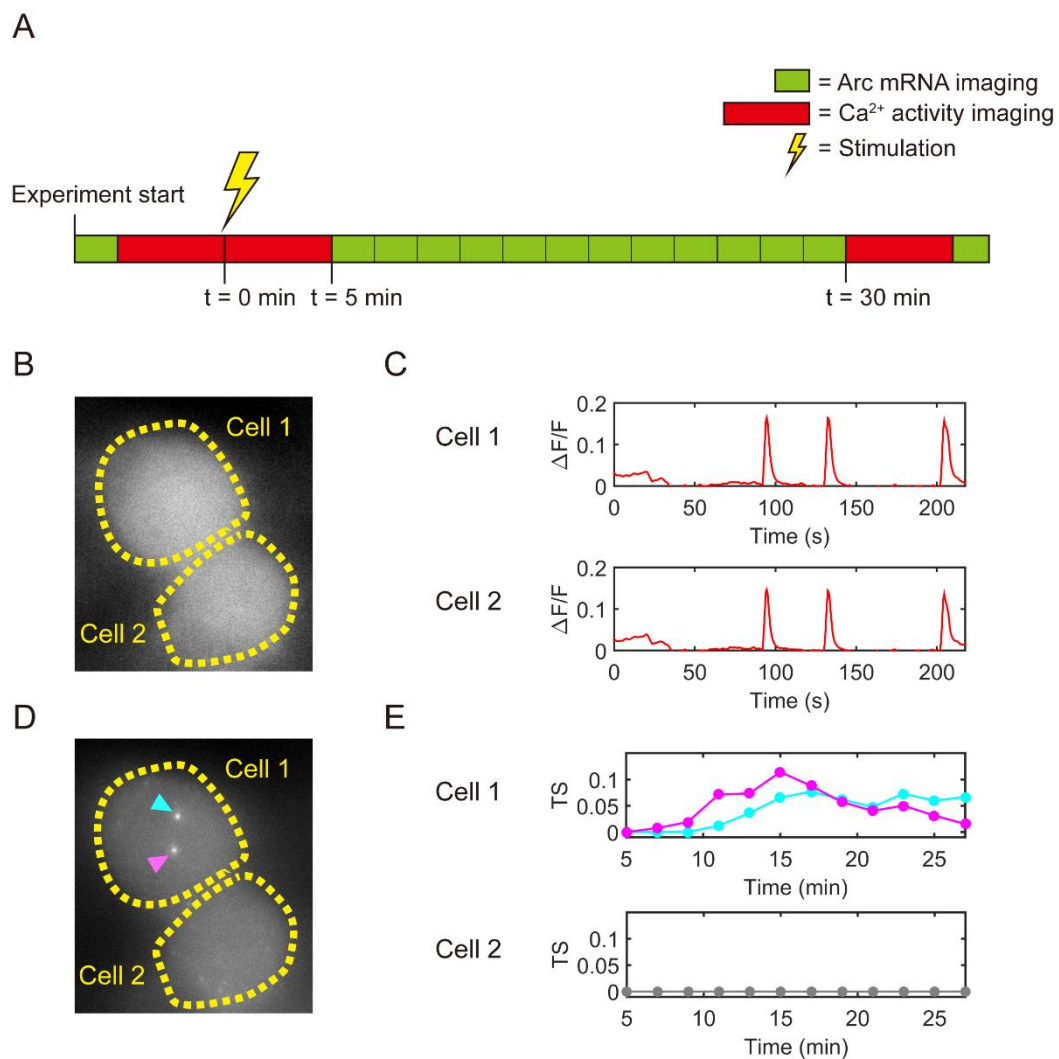


Figure 3.5 Ca²⁺ activity and Arc transcription from live neurons were observed by dual-color imaging. (A) Experiment scheme of imaging both Ca²⁺ activity and Arc transcription from the same neuron. One green block represents one z-stack imaging through the nucleus to detect Arc transcription sites in the GFP channel. One red block represents continuous Ca²⁺ activity imaging at the single plane of the nucleus for ~5 min in the Cy3 channel. The same neuron was monitored before and

after the stimulation by 50 μ M bicuculline. **(B)** Representative Ca^{2+} activity snapshot from the Cy3 channel. **(C)** Synchronized Ca^{2+} activities measured from the soma (area within dashed line) of neuron 1 (upper panel) and neuron 2 (lower panel) 5 min after bicuculline stimulation. **(D)** Representative image of Arc transcription snap shot in the same neurons as shown in **(B)**. Transcription from both alleles in neuron 1 (cyan and magenta arrow heads) versus no transcription from neither allele in neuron 2. **(E)** Time-course plot of Arc transcription activity in neuron 1 (upper panel) and neuron 2 (lower panel).

To quantitatively investigate the correlation between Ca^{2+} activity and Arc transcription activity, we designed paradigm to image both kinds of activities. Because Ca^{2+} activity imaging needs fast frame intervals at single z plane, while Arc transcription activity needs z stack images which cover the whole nucleus, we couldn't image both activities literally simultaneous. But we concluded it is sufficient to image both activities separately in time but from the same neuron in our experimental paradigm (Figure 3.5A). We've shown that Ca^{2+} activity persists during incubation with bicuculline which strengthens our argument (Figure 3.1). Therefore, we are pretty sure that Ca^{2+} activity also persists during the time while we are only imaging Arc transcription activity. We could observe stimulation with bicuculline induced synchronized somatic Ca^{2+} spikes in neurons within the field of view (Figure 3.5B and C), with frequency ranging from 0.008 to 0.04 Hz (0.019

± 0.009 Hz in average) and duration (full width at half maximum) ranging from 2 to 14 s (6.4 ± 3.2 s in average).

Upon exposure to bicuculline, all neurons showed an immediate increase in the frequency of Ca^{2+} activity, but only 43% exhibited induction of Arc transcription within ~ 30 min of stimulation (Figure 3.5D and E). Transcriptional initiation time was also highly heterogeneous, ranging from a few minutes to longer than 20 min after stimulation, although Ca^{2+} activity persisted during the entire duration of bicuculline treatment (Figure 3.6 and 3.7). Also, both alleles did not always transcribe Arc together, suggesting that intrinsic noise of transcription process exists. The burst width and frequency of Ca^{2+} activity were compared between neurons with and without Arc transcription within 30 min after bicuculline stimulation (Figure 3.8); no significant difference was observed ($P_{\text{ks}} > 0.05$, Kolmogorov-Smirnov test). These results indicate that although elevated Ca^{2+} activity is a prerequisite for Arc transcription, it is not always sufficient in inducing an active transcriptional burst.

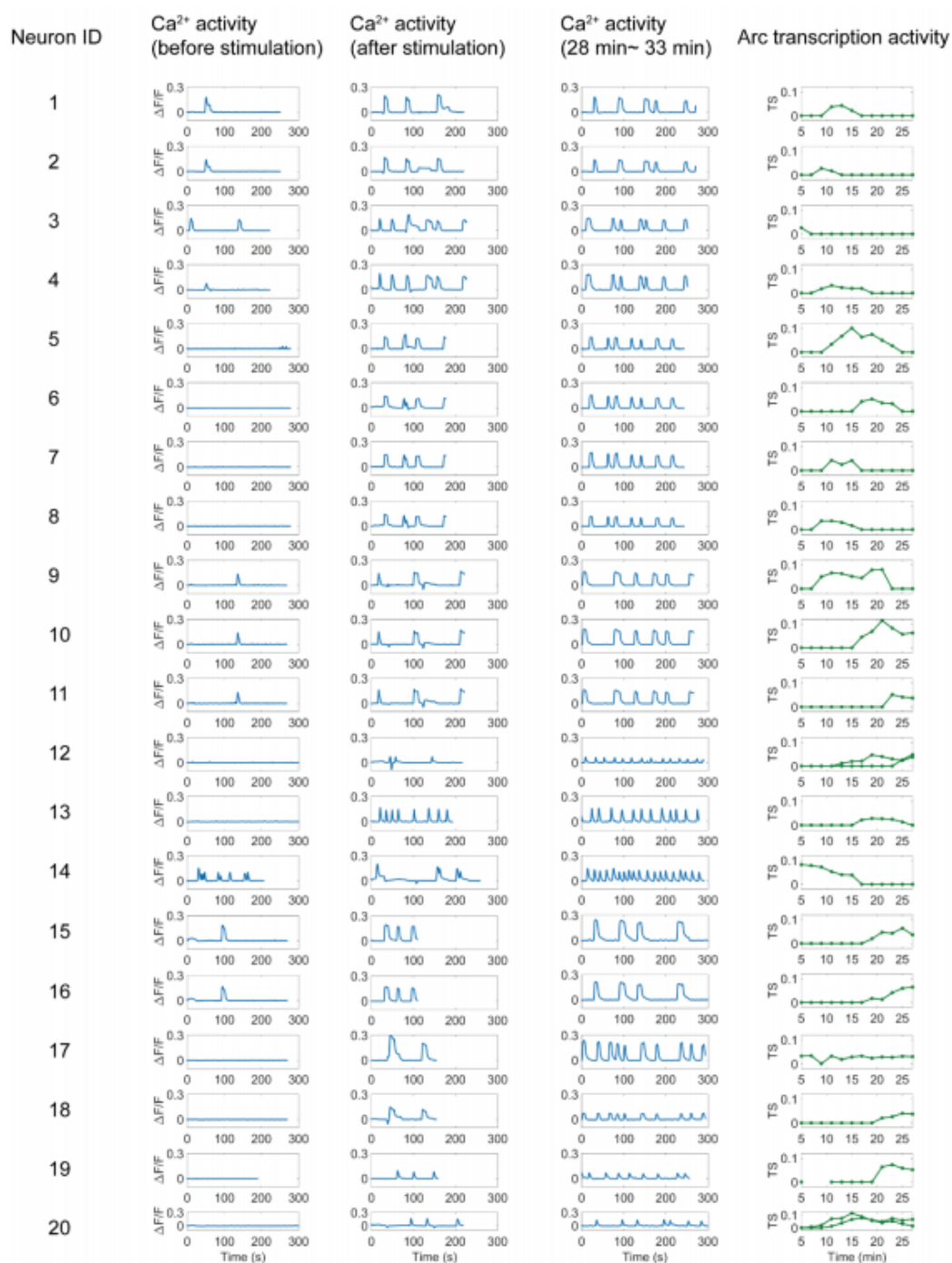


Figure 3.6 Plot of Ca²⁺ activity and Arc transcription activities. Data set of

neurons with Arc transcription. First column represents Ca^{2+} activity before stimulation (basal condition). Second column represents Ca^{2+} activity within 5 min after bicuculline application except for neuron 19. In case of neuron 19, Ca^{2+} activity of second column was measured 7-10.5 min after stimulation. Therefore, Arc transcription image for neuron 19 was taken from 11 min after stimulation. Third column represents Ca^{2+} activity 28-33 min after stimulation. The last column corresponds to time-lapse Arc transcription activity during 5-27 min after stimulation.

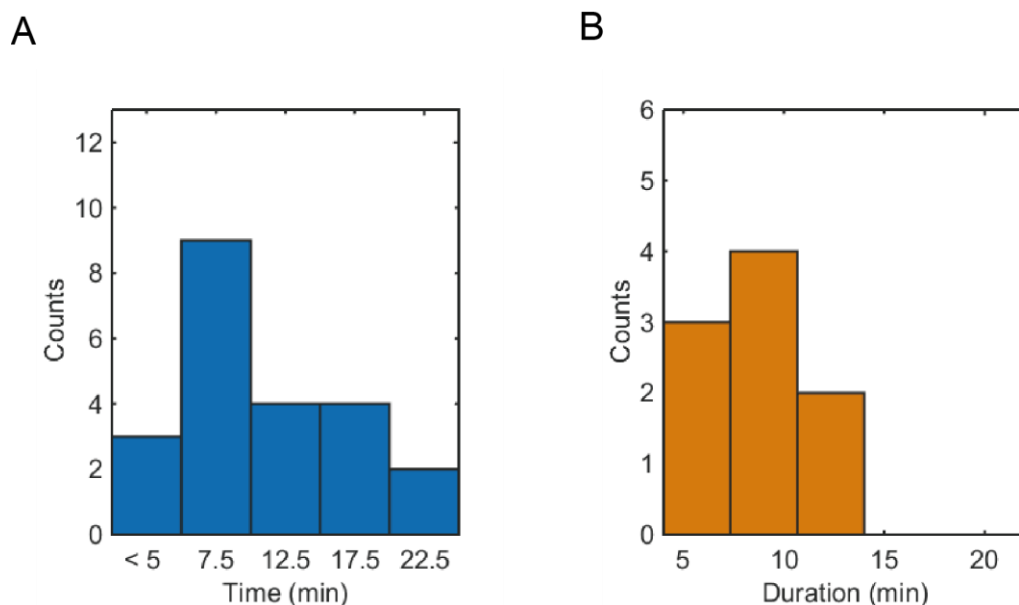


Figure 3.7 Heterogenous distribution of initiation and duration of Arc transcription bursts. (A) Distribution of first initiation of Arc transcription after bicuculline stimulation (n=22 transcription sites). **(B)** Distribution of Arc transcriptional burst duration after bicuculline stimulation (n=9 transcription sites).

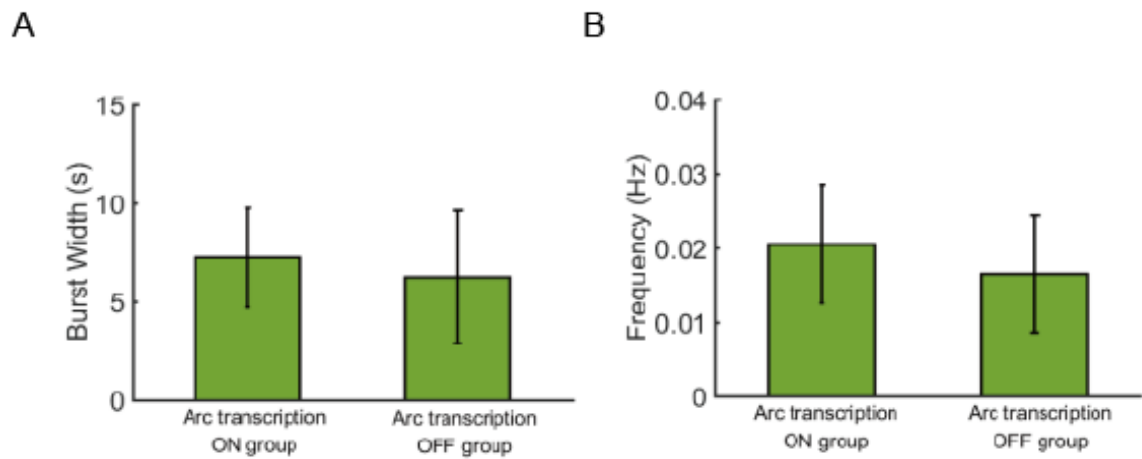


Figure 3.8 Comparison of somatic Ca²⁺ spikes between two groups of neurons with or without Arc transcription within 30 min after bicuculline stimulation.

(A) Comparison of the average full width at half maximum (FWHM) of Ca²⁺ spikes. No significant difference was observed between two groups ($P_{ks} > 0.05$, Kolmogorov –Smirnov test). **(B)** Comparison of average burst frequency of Ca²⁺ spikes. No significant difference was observed between two groups ($P_{ks} > 0.05$, Kolmogorov –Smirnov test). Error bars represent SD (n = 20 neurons for Arc transcription ON group, and n = 26 neurons for Arc transcription OFF group).

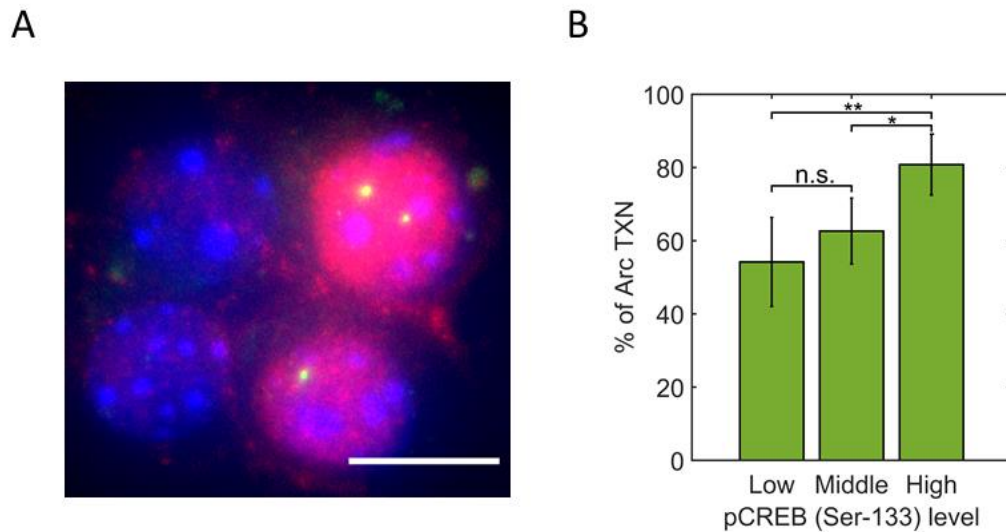


Figure 3.9 Neurons with high pCREB levels have high probability of having Arc transcription sites. (A) Representative IF-smFISH image of Arc transcription (green) and phosphorylated CREB (red) in the nucleus (DAPI, blue). Scale bar represents 10 μm . (B) Probability of having Arc transcription sites. Neurons were grouped by pCREB levels in the nucleus. (**, $P < 0.01$; *, $P < 0.05$; Two-tailed t-test). Total of 203 neurons were imaged from four independent experiments. Error bars represent SEM.

We next investigated possible mechanisms underlying this heterogeneity in the Arc transcriptional response to stimulation. The transcription factor CREB has been shown to play a key role in immediate early gene activation [14]. To evaluate the levels of nuclear phosphorylated CREB (pCREB, ser-133 residue) in Arc-

transcribing cells, immunofluorescence of pCREB along with smFISH for Arc mRNA was performed (Figure 3.9). A correlation was apparent when comparing the levels of nuclear pCREB and Arc transcription: there was a higher probability of Arc transcription in neurons with higher pCREB expression. These results indicated that although elevated Ca^{2+} spiking was a pre-requisite for Arc transcription, it was not sufficient in inducing an active transcriptional burst. Other factors such as the amplitude of nuclear Ca^{2+} signal [15], the absolute amount of CREB [16, 17], and the intrinsic noise in transcription machinery [18] may also play important roles in determining the efficiency of the transcriptional response to stimulation.

3.4 Conclusion and Outlook

Arc transcription site has been considered and used as a marker for neural activity, here we find out this one-to-one correspondence might not hold tightly especially in short timescale. However, this might be a difference arising from our cultured neuron system and *in vivo* system. Therefore, I think it is important to evaluate one-to-one correspondence relationship between Arc transcription and Ca^{2+} activity in *in vivo* context also. We also showed there might be difference in threshold to induce Arc transcription between neurons to neurons as there was positive correlation between pCREB level and Arc transcription site level. We could observe some refractory period of when Ca^{2+} activity is present, but no Arc transcription

activity [19]. Alcino Silva's lab suggested that C-C chemokine receptor 5 (CCR5) might act as a key molecule for the refractory period of neuronal plasticity enabling exclusive allocation of engram [20]. The further investigation of the relationship between CCR5 and Arc transcription would be intriguing. Next, in this study we used only bicuculline stimulation which we couldn't manipulate the frequency or amplitude of the input Ca^{2+} spikes. By using electrical field stimulation or optogenetics, controlling pattern of input Ca^{2+} activity and observing Arc transcription dynamics would be important for more concrete understanding about the mechanism of Arc transcription.

3.5 References

1. Cole, A. J., Saffen, D. W., Baraban, J. M., & Worley, P. F. (1989). Rapid increase of an immediate early gene messenger RNA in hippocampal neurons by synaptic NMDA receptor activation. *Nature*, 340(6233), 474-476.
2. Guzowski, J. F., McNaughton, B. L., Barnes, C. A., & Worley, P. F. (1999). Environment-specific expression of the immediate-early gene *Arc* in hippocampal neuronal ensembles. *Nature neuroscience*, 2(12), 1120-1124.
3. Zhai, S., Ark, E. D., Parra-Bueno, P., & Yasuda, R. (2013). Long-distance integration of nuclear ERK signaling triggered by activation of a few dendritic spines. *Science*, 342(6162), 1107-1111.
4. Wiegert, J. S., Bengtson, C. P., & Bading, H. (2007). Diffusion and not active transport underlies and limits ERK1/2 synapse-to-nucleus signaling in hippocampal neurons. *Journal of Biological Chemistry*, 282(40), 29621-29633.
5. Farris, S., & Dudek, S. M. (2015). From Where? Synaptic Tagging Allows the Nucleus Not to Care. In *Synaptic Tagging and Capture* (pp. 143-153). Springer, New York, NY.
6. Hardingham, G. E., Arnold, F. J., & Bading, H. (2001). Nuclear calcium signaling controls CREB-mediated gene expression triggered by synaptic activity. *Nature neuroscience*, 4(3), 261-267.
7. Bitto, H., Deisseroth, K., & Tsien, R. W. (1996). CREB phosphorylation and dephosphorylation: a Ca²⁺-and stimulus duration-dependent switch for hippocampal gene expression. *Cell*, 87(7), 1203-1214.

8. Deisseroth, K., Bitto, H., & Tsien, R. W. (1996). Signaling from synapse to nucleus: postsynaptic CREB phosphorylation during multiple forms of hippocampal synaptic plasticity. *Neuron*, 16(1), 89-101.
9. Tao, X., Finkbeiner, S., Arnold, D. B., Shaywitz, A. J., & Greenberg, M. E. (1998). Ca²⁺ influx regulates BDNF transcription by a CREB family transcription factor-dependent mechanism. *Neuron*, 20(4), 709-726.
10. Eliscovich, C., Shenoy, S. M., & Singer, R. H. (2017). Imaging mRNA and protein interactions within neurons. *Proceedings of the National Academy of Sciences*, 114(10), E1875-E1884.
11. Jaqaman, K., Loerke, D., Mettlen, M., Kuwata, H., Grinstein, S., Schmid, S. L., & Danuser, G. (2008). Robust single-particle tracking in live-cell time-lapse sequences. *Nature methods*, 5(8), 695.
12. Patel, T. P., Man, K., Firestein, B. L., & Meaney, D. F. (2015). Automated quantification of neuronal networks and single-cell calcium dynamics using calcium imaging. *Journal of neuroscience methods*, 243, 26-38.
13. Schneider, C. A., Rasband, W. S., & Eliceiri, K. W. (2012). NIH Image to ImageJ: 25 years of image analysis. *Nature methods*, 9(7), 671-675.
14. Sheng, M., McFadden, G., & Greenberg, M. E. (1990). Membrane depolarization and calcium induce c-fos transcription via phosphorylation of transcription factor CREB. *Neuron*, 4(4), 571-582.
15. Kawashima, T., Kitamura, K., Suzuki, K., Nonaka, M., Kamijo, S., Takemoto-Kimura, S., ... & Bitto, H. (2013). Functional labeling of neurons and their projections using the synthetic activity-dependent promoter E-SARE. *Nature methods*, 10(9), 889.

16. Han, J. H., Kushner, S. A., Yiu, A. P., Cole, C. J., Matynia, A., Brown, R. A., ... & Josselyn, S. A. (2007). Neuronal competition and selection during memory formation. *science*, 316(5823), 457-460.
17. Zhou, Y., Won, J., Karlsson, M. G., Zhou, M., Rogerson, T., Balaji, J., ... & Silva, A. J. (2009). CREB regulates excitability and the allocation of memory to subsets of neurons in the amygdala. *Nature neuroscience*, 12(11), 1438.
18. Elowitz, M. B., Levine, A. J., Siggia, E. D., & Swain, P. S. (2002). Stochastic gene expression in a single cell. *Science*, 297(5584), 1183-1186.
19. Das, S., Moon, H. C., Singer, R. H., & Park, H. Y. (2018). A transgenic mouse for imaging activity-dependent dynamics of endogenous Arc mRNA in live neurons. *Science advances*, 4(6), eaar3448.
20. Zhou, M., Greenhill, S., Huang, S., Silva, T. K., Sano, Y., Wu, S., ... & Lee, Y. S. (2016). CCR5 is a suppressor for cortical plasticity and hippocampal learning and memory. *Elife*, 5, e20985.

4. Dynamics of Arc mRNA transport in dendrite of live hippocampal neurons

4.1 Introduction

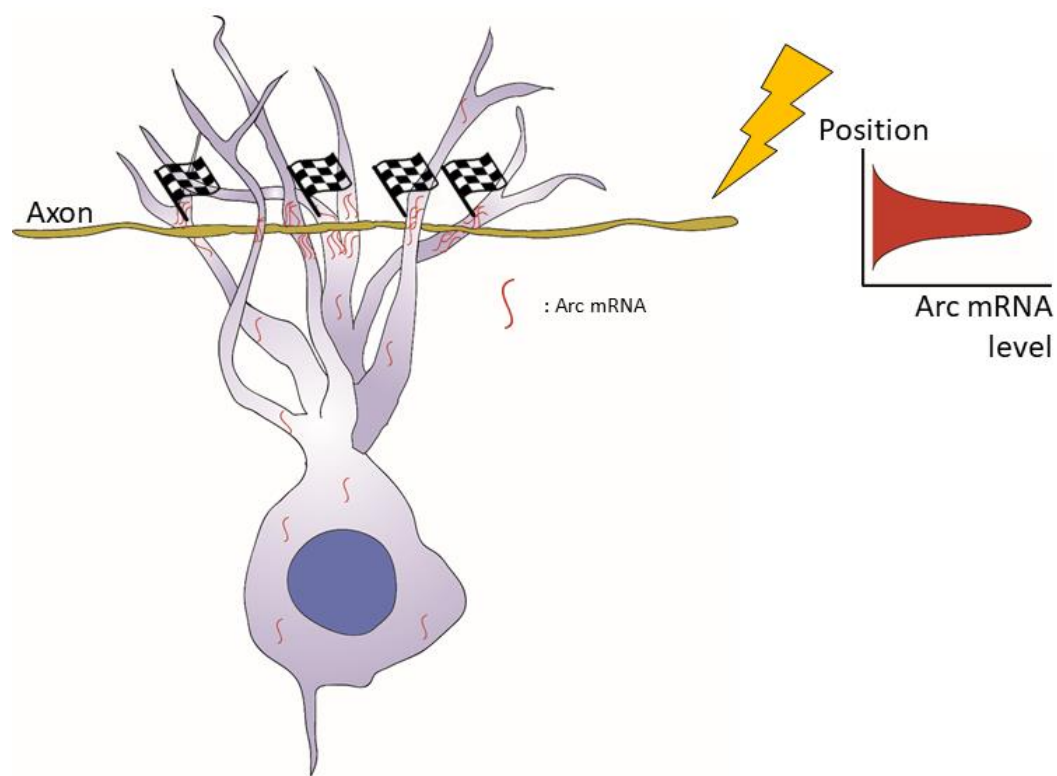


Figure 4.1 Selective localization of Arc mRNA to activated synapses.

This figure summarizes one of key findings of reference [1]. LTP inducing high

frequency stimulus was given to yellow neuron (Here, only axon part of yellow neuron is shown.). Arc mRNAs are induced from purple neuron as purple neuron gets excited by receiving inputs from synapses formed with yellow neuron. After continuous delivery of stimulation for 2 hours, Arc mRNAs are localized near highly activated synapse between purple and yellow neurons.

Synaptic activation causes the Arc mRNA to selectively localize near activated postsynaptic sites on dendrites (Figure 4.1.) [1]. This localization is dependent on NMDA receptor activation and 3'UTR of Arc mRNA [1, 2]. Recently, a question of whether Arc mRNA is the unique mRNA that localizes to the dendrite in activity dependent manner was asked. By using laser microdissection to accurately dissect out dendrites, and performing microarray analysis, this question was answered [3]. *Egr2*, *Egr4*, *Fosb*, *Nr4a3*, *RM2*, *Homer1a* and *BDNF* transcripts were also shown to undergo activity dependent localization to dendrite. However, the fold difference between before stimulation and after stimulation was the biggest in the case of gene *Arc*. Arc mRNA is a target of nonsense mediated decay (NMD) [4]. Therefore, Arc mRNAs undergo degradation after initial round of translation. Also, Arc mRNA undergoes neural activity dependent translation [5-7]. Dr. Steward's group showed that neural activity dependent translation and thus degradation are both required for selective localization phenomena of Arc mRNA [8]. Recently, Arc protein's oligomerization and exosome-like behavior to

shuttle mRNAs including Arc mRNA for intercellular communication was discovered [9, 10]. And this oligomerization of Arc is regulated by phosphorylation action of CamkII [11]. It would be interesting question to probe the relationship between these Arc exosome and Arc mRNA localization phenomena. Next, it was reported that Arc mRNA localization phenomena in brain slice experiment was less reliable on mouse compared to rats [2]. The author explains this might be due to some anatomical difference on perforant path between mouse and rat. Every experiment described above was performed on fixed cells. Therefore, most of the studies were focused on the final destination of Arc mRNA not the process of localization. In order to study process of localization, live cell imaging is necessary. Dr. Steward's group used exogenous reporter with 3'UTR of Arc mRNA to observe the dynamics of exogenous Arc mRNA in the dendrite [12, 13]. They've shown bidirectional movement and speed ranged between 6~60 $\mu\text{m/s}$. Also, reporter mRNAs could dock at the end of dendritic spine bases. However, exogenous reporter with only 3'UTR of Arc mRNA might have some differences from the endogenous full transcript. Here, we observed and characterized transport dynamics of tagged endogenous Arc mRNA in hippocampal neuron culture.

4.2 Materials and Methods

Hippocampal neuron culture

Hippocampi were dissected out from postnatal day 1(P1) pups from Arc^{P/+} heterozygous x heterozygous mice. Hippocampal neurons were isolated as described before [9]. Dissected hippocampi were kept at ice cold neural dissection solution (NDS) (10 mM Hank's balanced salt solution (HBSS) (Gibco, cat No. 14185) and 19 mM HEPES (Gibco, cat. No. 15630-080) in water). After collection, hippocampi were digested with 0.25% Trypsin in NDS at 37° C for 15 mins, followed by trituration. After trituration, trypsin was removed and media was changed to plating medium (PM) (10% FBS heat inactivated (Gibco, cat. No. 10082-147), 1x Glutamax (Gibco, cat. No. 35050-061) and 0.1 mg/ml Primocin (Invivogen, cat. No. ant-pm-1) in Neurobasal A medium (Gibco, cat. No. 10888-022)). Hemocytometer was used to count the density of hippocampal neurons. Hippocampal neurons were plated onto overnight PDL-coated Mattek dishes with the appropriate density (200 µl of 425,000 cells/ml). After 4 hours incubation in the 37° C, 5% CO₂ incubator, 1.8 ml of equilibrated B27 medium (1x B27 (Gibco, cat. No. 17504-044), 1x Glutamax (Gibco, cat. No. 35050-061) and 0.1 mg/ml primocin (Invivogen, cat. No. ant-pm-1) in Neurobasal A medium (Gibco, cat. No. 10888-022)) was added to each dish. Every 7 days after seeding, gently add 300 µl of equilibrated B27 medium to the cells. Because neurons are too vulnerable, it is recommended to refrain from taking neurons out of incubator.

Preparation of viruses

Coding sequences for NLS-stdPCP-stdGFP were cloned into AAV expression vectors. The synonymous versions of PCP (stdPCP) and GFP (stdGFP) were designed based on previously described coat proteins and fluorescent proteins (32). Serotype 2/1 AAV vector for expression of hSyn-NLS-stdPCP-stdGFP was generated using the AAV Helper-Free System (Agilent Technologies). The final concentration of AAV infection was $\sim 10^9$ genome copies per ml (GC/ml). After infection with AAV, no media change was performed, and NGM was added to the cultures every 3 days.

Imaging dendritic transport of Arc mRNA

Neurons were infected with AAV-hSyn-NLS-stdPCP-stdGFP on DIV 11-13. Live-cell imaging experiments were performed on DIV 14-15. For bicuculline washout condition, neurons were stimulated with 50 μ M bicuculline in NGM and placed in 37°C, 5% CO₂ incubator for 20 min. After washing with warmed HBS media, neurons were brought to the wide-field fluorescence microscope described above and incubated at 37°C for 20 min until the microscope system became equilibrated. During equilibration, several fields of view which contained a few dendrites were selected. Then each site was imaged at 5 Hz for 1 min during 40-60 min after the onset of bicuculline stimulation. In order to inhibit action potentials, a sodium channel blocker TTX was used. To inhibit NMDA and AMPA receptors, APV and

CNQX were used, respectively. For bicuculline washout + TTX and bicuculline washout + TTX + APV + CNQX conditions, Arc transcription was also induced by 50 μ M bicuculline for 20 min. Then, neurons were washed and incubated with 1.5 μ M TTX or 1.5 μ M TTX + 300 μ M APV + 10 μ M CNQX in HBS media. All the following procedures and parameters for imaging of bicuculline washout + TTX condition and bicuculline washout + TTX + APV + CNQX condition were the same as bicuculline washout condition.

Image analysis

Movements of Arc mRNAs in dendrites were analyzed based on kymographs generated by ImageJ. The run phase was defined as movement with displacement larger than 1.5 μ m. The start point and the end point of run phase were annotated manually on kymographs and used to calculate the displacement and the velocity of each particle. The average and standard error of mean (SEM) were calculated from 5 independent experiments for each condition in **Figure 4.4B, D, and E**. Two-tailed t-test was used to determine the P-values. For **Figure 4.4F**, the probability density functions (PDFs) of run velocity were also obtained from 5 independent experiments for each condition. Kolmogorov-Smirnov test was used to measure the significance of difference between velocity PDFs.

4.3 Results and Discussion

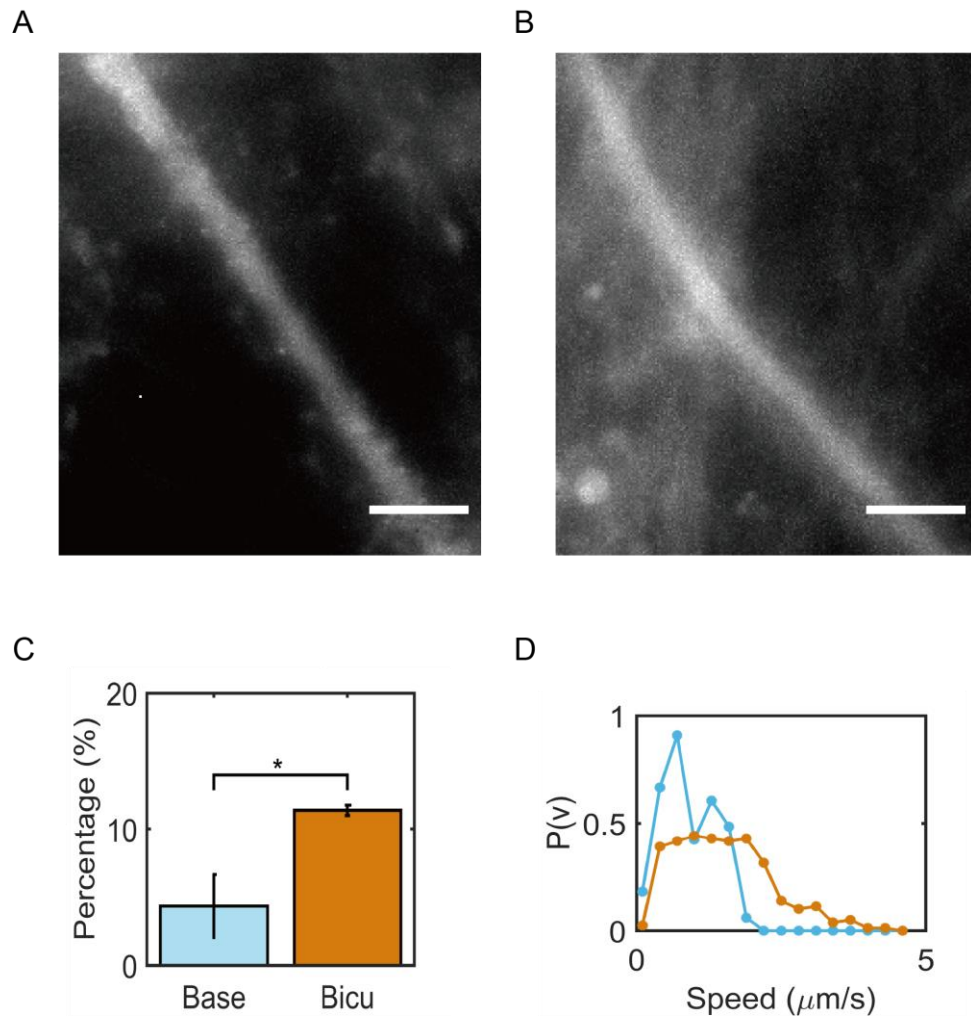


Figure 4.2 False positive tdPCPtdGFP aggregates in dendrite.

(A) A representative image of false positive particles in dendrite from tdPCP-tdGFP infected wild-type neuron. (B) A representative image of dendrite from stdPCP-stdGFP infected wild-type neuron. False positive particles are not observed. (C) Fraction of moving particles during 1 min observation in basal condition (Base) and bicuculline stimulated condition (Bicu). (*, $P < 0.05$; Two-tailed t-test) (D)

Probability distributions of speed of run phase in basal condition (cyan) and bicuculline stimulated condition (orange). (C) and (D) were analyzed from tdPCP-tdGFP infected Arc^{p/p} homozygous neuron culture which real Arc mRNAs and false positive particles are both present due to tdPCP-tdGFP aggregates. Scale bar represents 5 μm . Total of 1580 particles for bicuculline stimulated condition and 1454 particles from basal condition were analyzed from 5 independent experiments.

Although we observed that tdPCP-tdGFP tags Arc mRNA transcription sites (Figure 2.3), we tested whether tdPCP-tdGFP also tags Arc mRNA in the dendrite. As a negative control, we infected hSyn-NLS-tdPCP-tdGFP AAV virus to the wild-type neuron culture. As wild-type neuron doesn't have PBS sequence knocked-in, there should be no observable particles in GFP channel ideally. However, it was striking to observe mRNA like diffraction limited particles in the dendrite. These particles couldn't be distinguished from real Arc mRNAs by shape. If we didn't perform this negative control experiment, using tdPCP-tdGFP could lead to wrong data interpretation. For example, by analyzing motions of particles from tdPCP-tdGFP infected Arc^{p/p} homozygous neuron culture, we observed neural activity dependent increase in overall mobility (Figure 4.2). However, this phenomenon turned out to be not true in latter experiments which were performed by analyzing only true Arc mRNAs (Figure 4.5). As synonymous tandem mutated PCPGFP (stdPCP-stdGFP) didn't show false positives in wild-type neuron culture, we started

to use stdPCP-stdGFP construct for imaging the dendritic transport of Arc mRNAs.

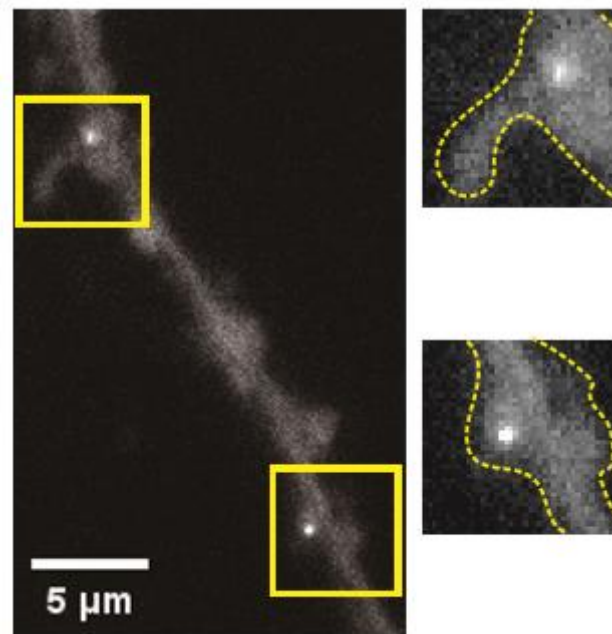


Figure 4.3 Tagged endogenous Arc mRNA localizes near dendritic spines.

A representative image of Arc mRNAs localized at the neck of a dendritic spine (upper right panel) and inside a spine (lower right panel).

Once transcribed, Arc mRNAs are transported to the dendrites and localize at activated synapses [1]. In Arc^{P/P} neurons, PBS-tagged endogenous Arc mRNAs were targeted to the dendrites and localized near dendritic spine necks and inside dendritic spines (Figure 4.3).

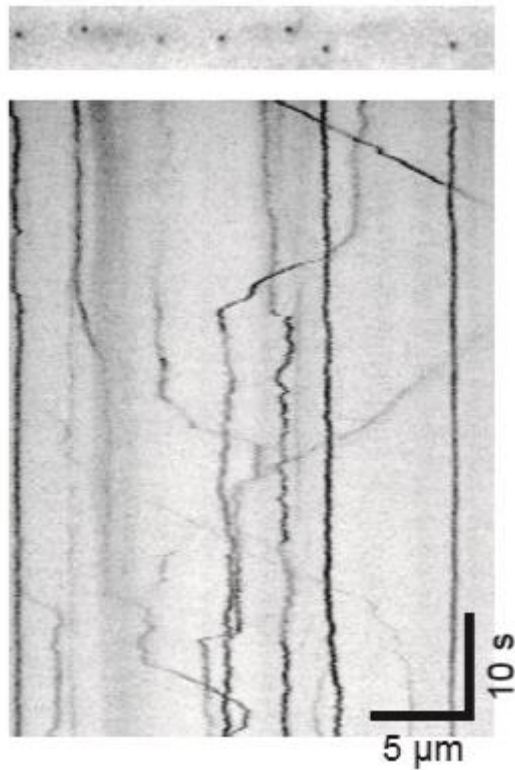


Figure 4.4 Representative kymograph of Arc mRNAs in dendrite.

Both stationary and actively moving Arc mRNAs are present in a dendrite. In this figure, nucleus is at the left side and not shown. Thus, Arc mRNA's run toward left direction is retrograde motion and toward right direction is anterograde direction. Constant velocity motion can be frequently observed.

We next performed single particle tracking to follow the movement of individual Arc mRNAs. The directed transport of Arc mRNA occurred in both anterograde and retrograde directions and was often interrupted by pauses (Figure 4.4), similar

to the previously reported transport behavior of β -actin mRNA [14, 15] and Arc 3' UTR reporter mRNA [12, 13]. The processive run with constant velocity resembled the movement of cargos transported by motor proteins. However, due to the mixed population of microtubules with two different orientations in proximal dendrites, classes of motor proteins that are involved in the transport of Arc mRNA couldn't be determined (Table 3).

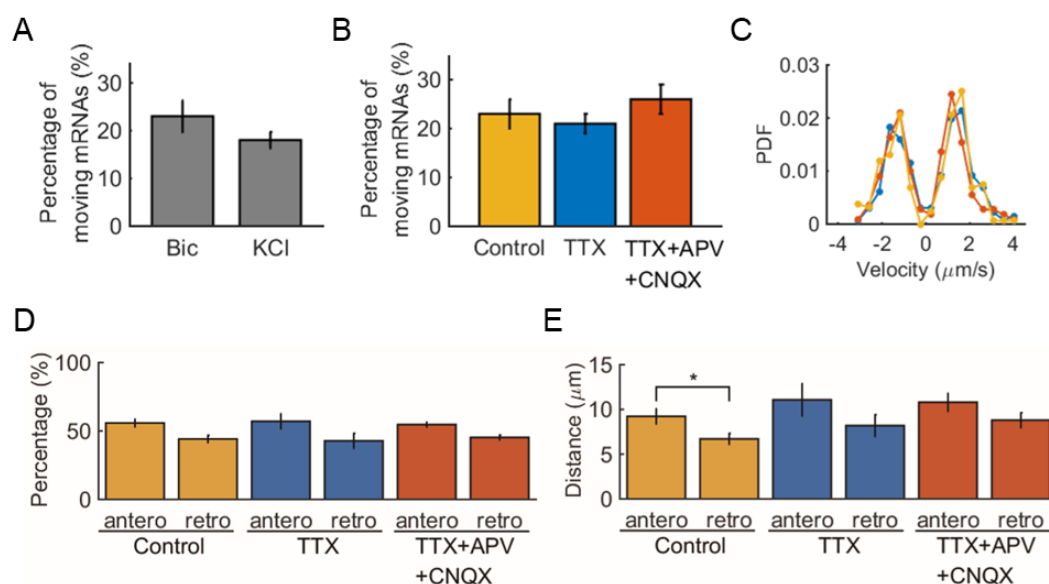


Figure 4.5 Transport dynamics of dendritic Arc mRNA. (A) Fraction of moving Arc mRNAs that displacement is more than 1.5 μm during 1 min of observation after bicuculline (Bic) and KCl stimulation (KCl). 510 and 141 mRNAs were analyzed for Bic and KCl conditions, respectively. (B) Fraction of moving Arc mRNAs in the bicuculline washout (Control), bicuculline washout + TTX (TTX) condition and bicuculline washout + TTX + APV + CNQX (TTX + APV + CNQX).

510, 427, and 549 mRNAs were analyzed for Control, TTX and TTX + APV + CNQX conditions, respectively. **(C)** Probability density function (PDF) of the velocity in Control (yellow), TTX (blue) and TTX + APV + CNQX (red) conditions, respectively. Velocity of run of Arc mRNA was similar among all conditions. **(D)** Percentage of anterograde (antero) and retrograde (retro) runs in all conditions. **(E)** Histogram of distance traveled by a single run movement in anterograde and retrograde directions for Control, TTX and TTX + APV + CNQX conditions, respectively. (*, $P < 0.05$; Two-tailed t-test). For **(B)-(E)**, total of 173, 146 and 212 runs from 5 independent experiments were analyzed for Control, TTX and TTX + APV + CNQX conditions, respectively. Error bars represent SEM.

The fraction of mobile Arc mRNAs that moved longer than $1.5 \mu\text{m}$ during 1 min of observation was $23 \pm 3\%$ (mean \pm SEM) upon bicuculline stimulation and $18 \pm 2\%$ upon KCl depolarization, showing no significant difference between the two stimulation paradigms ($P = 0.35$, two-tailed t-test) (Figure 4.5A).

Since neuronal activity is crucial for the induction of Arc mRNA, we assessed the effect of neuronal activity on transport dynamics of Arc mRNA. A cocktail of TTX, NMDA receptor antagonist (APV) and AMPA receptor antagonist (CNQX) was used to block both evoked and spontaneous activity. Dendritic transport of newly synthesized Arc mRNAs was imaged in the proximal dendrites 20-40 min after

bicuculline treatment and washout (control), bicuculline washout and TTX treatment (TTX), and bicuculline wash out followed by TTX, APV, and CNQX treatment (TTX + APV + CNQX). Surprisingly, there was no significant difference in the fraction of actively moving Arc mRNA among all conditions. The percentage of mobile Arc mRNA was $23 \pm 3\%$ (mean \pm SEM) in control condition, $21 \pm 3\%$ in TTX condition and $26 \pm 3\%$ in TTX + APV + CNQX condition (Figure 4.5B). The motion of Arc mRNA was further analyzed by segmenting the kymographs (Figure 4.4) into two states, run and rest/pause phases, where movement longer than $1.5 \mu\text{m}$ was defined as a run phase. The velocity probability density functions (PDFs) of run phases were also similar across the three conditions, suggesting that the run phase occurs independent of synaptic activity (Figure 4.5C; $P_{\text{ks}} > 0.07$ for all three pairs, Kolmogorov –Smirnov test). The speed of a single run was $1.5 \pm 0.7 \mu\text{m/s}$, $1.4 \pm 0.7 \mu\text{m/s}$ and $1.6 \pm 0.7 \mu\text{m/s}$ (mean \pm SD) for each condition respectively, which indicates that the active transport of Arc mRNAs on microtubules was not altered by inhibiting neuronal activity. This was irrespective of whether the runs were in anterograde or retrograde directions, since the percentage of run events in either direction was similar in all conditions (Figure 4.5D). Interestingly, the average distance traveled by a single anterograde run ($9.2 \pm 0.8 \mu\text{m}$) was significantly longer than that by a retrograde run ($6.7 \pm 0.6 \mu\text{m}$) under stimulated condition (Figure 4.5E ; $P < 0.05$, two-tailed t-test). This suggested that the slightly biased walk with a longer run phase to the anterograde direction possibly mediates

the delivery of Arc mRNAs to the distal dendrites. However, neuronal activity did not play a significant role in changing the transport velocities of Arc mRNA unlike transport behavior of mitochondria.

	Speed	Organism	<i>In vitro / In vivo</i>	Reference
Cytoplasmic Dynein	0.1 $\mu\text{m/s}$	<i>Yeast</i>	<i>In vitro</i>	[22]
	1-3 $\mu\text{m/s}$	<i>Chicken, rat, human</i>	<i>In vitro</i>	[23-27]
Axonemal Dynein	30 $\mu\text{m/s}$	<i>Chlamydomonas reinhardtii</i>	<i>In vitro</i>	[28]
KIF1A	1.8 $\mu\text{m/s}$	<i>rat</i>	<i>In vitro</i>	[29]
KIF5C	0.9 $\mu\text{m/s}$	<i>rat</i>	<i>In vitro</i>	[29]
KIF17	1.3 $\mu\text{m/s}$	<i>human</i>	<i>In vivo</i>	[30]
KIF18b	0.6 $\mu\text{m/s}$	<i>human</i>	<i>In vivo</i>	[31]

Table 3. Previously measured speeds of motor proteins

4.4 Conclusion and outlook

Here we could observe transport dynamics of tagged endogenous Arc mRNAs in live hippocampal neurons. Similar to reported transport behavior of β -actin mRNAs [14, 15], Arc mRNAs also showed bidirectional motion interrupted by rests. Occurrence of anterograde and retrograde walk phase were similar ~50%. However, single walk was longer in anterograde direction. These mobility properties were not perturbed by global silence of neural activity with sodium channels and ionotropic

glutamate receptors blockade. While somatic Ca^{2+} activity is necessary for the induction of Arc mRNA, the random walk-like active transport of Arc mRNA can proceed without neuronal firing. This result indicates that dendritic transport of mRNA is distinct from trafficking of mitochondria which its speed is coupled to synaptic activity [16]. For example, TTX treatment increases the speed of mitochondria whereas KCl depolarization decreases the speed [17]. Mitochondria-kinesin adaptor protein Miro1 is a Ca^{2+} sensor which mediates ionotropic glutamate receptor dependent localization of mitochondria [18, 19]. Although adaptor proteins that link Arc mRNA to motor proteins are still need to be identified, our results provide a new insight and approach to understand the microscopic characteristics of Arc mRNA transport to the activated synapses. The activity dependent localization suggests intense neural activity makes Arc mRNAs to stop. However, we couldn't observe neural activity-dependent anchoring of Arc mRNAs. Several possibilities that need to be tested still exist. One, in this study we silenced the global activity of neuron, may be the gradient of activity is needed for Arc mRNA anchoring. This can be tested with glutamate uncaging as in the case of previous study with β -actin mRNAs [20]. Two, bicuculline may induce transcription of Arc mRNA but doesn't trigger LTP. From the previous study of testing Arc mRNA localization to activated synapses, LTP inducing stimuli was used. Therefore, LTP inducing stimuli might make Arc mRNA pause. Third, Arc mRNAs at distal dendrites might show more clear activity dependent anchoring. We only imaged

proximal dendrites in this study. Recently, Arc protein synthesis was reported to be regulated differentially in proximal and distal dendrites [21]. Fourth, overall degradation throughout the dendrite might help sculpting Arc mRNA localization pattern as suggested from recent paper [8].

4.5 References

1. Steward, O., Farris, S., Pirbhoy, P. S., Darnell, J., & Driesche, S. J. V. (2015). Localization and local translation of Arc/Arg3. 1 mRNA at synapses: some observations and paradoxes. *Frontiers in Molecular Neuroscience*, 7, 101.
2. Steward, O., Matsudaira Yee, K., Farris, S., Pirbhoy, P. S., Worley, P., Okamura, K., ... & Bito, H. (2018). Delayed degradation and impaired dendritic delivery of intron-lacking EGFP-Arc/Arg3. 1 mRNA in EGFP-Arc transgenic mice. *Frontiers in molecular neuroscience*, 10, 435.
3. de Solis, C. A., Morales, A. A., Hosek, M. P., Partin, A. C., & Ploski, J. E. (2017). Is Arc mRNA unique: a search for mRNAs that localize to the distal dendrites of dentate gyrus granule cells following neural activity. *Frontiers in molecular neuroscience*, 10, 314.
4. Giorgi, C., Yeo, G. W., Stone, M. E., Katz, D. B., Burge, C., Turrigiano, G., & Moore, M. J. (2007). The EJC factor eIF4AIII modulates synaptic strength and neuronal protein expression. *Cell*, 130(1), 179-191.
5. Na, Y., Park, S., Lee, C., Kim, D. K., Park, J. M., Sockanathan, S., ... & Worley, P. F. (2016). Real-time imaging reveals properties of glutamate-induced Arc/Arg 3.1 translation in neuronal dendrites. *Neuron*, 91(3), 561-573.
6. Park, S., Park, J. M., Kim, S., Kim, J. A., Shepherd, J. D., Smith-Hicks,

- C. L., ... & Huganir, R. L. (2008). Elongation factor 2 and fragile X mental retardation protein control the dynamic translation of Arc/Arg3.1 essential for mGluR-LTD. *Neuron*, 59(1), 70-83.
7. Waung, M. W., Pfeiffer, B. E., Nosyreva, E. D., Ronesi, J. A., & Huber, K. M. (2008). Rapid translation of Arc/Arg3.1 selectively mediates mGluR-dependent LTD through persistent increases in AMPAR endocytosis rate. *Neuron*, 59(1), 84-97.
 8. Farris, S., Lewandowski, G., Cox, C. D., & Steward, O. (2014). Selective localization of arc mRNA in dendrites involves activity-and translation-dependent mRNA degradation. *Journal of Neuroscience*, 34(13), 4481-4493.
 9. Ashley, J., Cordy, B., Lucia, D., Fradkin, L. G., Budnik, V., & Thomson, T. (2018). Retrovirus-like Gag protein Arc1 binds RNA and traffics across synaptic boutons. *Cell*, 172(1-2), 262-274.
 10. Pastuzyn, E. D., Day, C. E., Kearns, R. B., Kyrke-Smith, M., Taibi, A. V., McCormick, J., ... & Briggs, J. A. (2018). The neuronal gene arc encodes a repurposed retrotransposon gag protein that mediates intercellular RNA transfer. *Cell*, 172(1-2), 275-288.
 11. Zhang, W., Chuang, Y. A., Na, Y., Ye, Z., Yang, L., Lin, R., ... & Leahy, D. J. (2019). Arc Oligomerization Is Regulated by CaMKII Phosphorylation of the GAG Domain: An Essential Mechanism for Plasticity and Memory Formation. *Molecular cell*, 75(1), 13-25.
 12. Dynes, J. L., & Steward, O. (2007). Dynamics of bidirectional transport

of Arc mRNA in neuronal dendrites. *Journal of Comparative Neurology*, 500(3), 433-447

13. Dyne, J. L., & Steward, O. (2012). Arc mRNA docks precisely at the base of individual dendritic spines indicating the existence of a specialized microdomain for synapse-specific mRNA translation. *Journal of Comparative Neurology*, 520(14), 3105-3119.
14. Park, H. Y., Lim, H., Yoon, Y. J., Follenzi, A., Nwokafor, C., Lopez-Jones, M., ... & Singer, R. H. (2014). Visualization of dynamics of single endogenous mRNA labeled in live mouse. *Science*, 343(6169), 422-424.
15. Song, M. S., Moon, H. C., Jeon, J. H., & Park, H. Y. (2018). Neuronal messenger ribonucleoprotein transport follows an aging Lévy walk. *Nature communications*, 9(1), 1-8.
16. Sheng, Z. H., & Cai, Q. (2012). Mitochondrial transport in neurons: impact on synaptic homeostasis and neurodegeneration. *Nature Reviews Neuroscience*, 13(2), 77-93.
17. Li, Z., Okamoto, K. I., Hayashi, Y., & Sheng, M. (2004). The importance of dendritic mitochondria in the morphogenesis and plasticity of spines and synapses. *Cell*, 119(6), 873-887.
18. MacAskill, A. F., Rinholm, J. E., Twelvetrees, A. E., Arancibia-Carcamo, I. L., Muir, J., Fransson, A., ... & Kittler, J. T. (2009). Miro1 is a calcium sensor for glutamate receptor-dependent localization of mitochondria at synapses. *Neuron*, 61(4), 541-555.

19. Ahmad, T., Mukherjee, S., Pattnaik, B., Kumar, M., Singh, S., Rehman, R., ... & Roy, S. S. (2014). Miro1 regulates intercellular mitochondrial transport & enhances mesenchymal stem cell rescue efficacy. *The EMBO journal*, 33(9), 994-1010.
20. Yoon, Y. J., Wu, B., Buxbaum, A. R., Das, S., Tsai, A., English, B. P., ... & Singer, R. H. (2016). Glutamate-induced RNA localization and translation in neurons. *Proceedings of the National Academy of Sciences*, 113(44), E6877-E6886.
21. Klein, M. E., Younts, T. J., Cobo, C. F., Buxbaum, A. R., Aow, J., Erdjument-Bromage, H., ... & Castillo, P. E. (2019). Sam68 Enables Metabotropic Glutamate Receptor-Dependent LTD in Distal Dendritic Regions of CA1 Hippocampal Neurons. *Cell reports*, 29(7), 1789-1799.
22. Reck-Peterson, S. L., Yildiz, A., Carter, A. P., Gennerich, A., Zhang, N., & Vale, R. D. (2006). Single-molecule analysis of dynein processivity and stepping behavior. *Cell*, 126(2), 335-348.
23. McKenney, R. J., Huynh, W., Tanenbaum, M. E., Bhabha, G., & Vale, R. D. (2014). Activation of cytoplasmic dynein motility by dynactin-cargo adapter complexes. *Science*, 345(6194), 337-341.
24. Mazumdar, M., Mikami, A., Gee, M. A., & Vallee, R. B. (1996). In vitro motility from recombinant dynein heavy chain. *Proceedings of the National Academy of Sciences*, 93(13), 6552-6556.
25. King, S. J., & Schroer, T. A. (2000). Dynactin increases the processivity of the cytoplasmic dynein motor. *Nature cell biology*, 2(1), 20-24.

26. Torisawa, T., Ichikawa, M., Furuta, A., Saito, K., Oiwa, K., Kojima, H., ... & Furuta, K. Y. (2014). Autoinhibition and cooperative activation mechanisms of cytoplasmic dynein. *Nature cell biology*, 16(11), 1118-1124.
27. Schlager, M. A., Hoang, H. T., Urnavicius, L., Bullock, S. L., & Carter, A. P. (2014). In vitro reconstitution of a highly processive recombinant human dynein complex. *The EMBO journal*, 33(17), 1855-1868.
28. Aoyama, S., & Kamiya, R. (2010). Strikingly fast microtubule sliding in bundles formed by *Chlamydomonas* axonemal dynein. *Cytoskeleton*, 67(6), 365-372.
29. Arpağ, G., Norris, S. R., Mousavi, S. I., Soppina, V., Verhey, K. J., Hancock, W. O., & Tüzel, E. (2019). Motor dynamics underlying cargo transport by pairs of kinesin-1 and kinesin-3 motors. *Biophysical journal*, 116(6), 1115-1126.
30. Cai, D., McEwen, D. P., Martens, J. R., Meyhofer, E., & Verhey, K. J. (2009). Single molecule imaging reveals differences in microtubule track selection between Kinesin motors. *PLoS Biol*, 7(10), e1000216.
31. Tanenbaum, M. E., Gilbert, L. A., Qi, L. S., Weissman, J. S., & Vale, R. D. (2014). A protein-tagging system for signal amplification in gene expression and fluorescence imaging. *Cell*, 159(3), 635-646.

5. Conclusion and Outlook

In this study, I investigated the dynamics of Arc mRNA transcription and transport in dendrites using Arc-PBS mouse which is a novel transgenic mouse enabling live cell imaging of single molecule Arc mRNA in real time.

In Chapter III, I investigated the correlation between Ca^{2+} activity and Arc transcription which is often believed to be in the relation of one to one correspondence. By directly measuring somatic Ca^{2+} spikes and Arc transcription from the same neuron, I observed only ~43 % of neurons transcribed Arc mRNA even after somatic Ca^{2+} bursts on hippocampal neuron culture. Next, by performing combined immunofluorescence with FISH, I showed that synchronized Ca^{2+} burst input triggered heterogenous phosphorylation of CREB and the positive correlation between pCREB level and Arc transcription. This study provided, for the first time, the direct real-time measurement of Ca^{2+} activity and Arc transcription from the same neuron and show the disparity of the relation from one to one correspondence. This result suggests that not only the external input but also internal state of the neuron matters for the induction of Arc transcription. Whether this is just an intrinsic limitation of Arc transcriptional machinery or it has actual function in the allocation of engram must be further studied *in vivo* or in the aspect of computational neuroscience.

In Chapter IV, I observed the real-time transport dynamics of Arc mRNAs in the dendrite. Single-molecule resolution enabled me to obtain trajectories of endogenous Arc mRNAs. The directed transport of Arc mRNA occurred in both anterograde and retrograde directions and was often interrupted by pauses similar to the previously reported transport behavior of β -actin mRNA. Next, I assessed the effect of neural activity on velocity, the occurrence of run in the anterograde or retrograde directions, and the portion of moving Arc mRNAs. Surprisingly, none of these parameters were affected by global inhibition of ionotropic neural activity. This study provided, for the first time, the direct observation of the endogenous Arc mRNA transport dynamics in the dendrite and suggests two key points. One, as trajectories of endogenous Arc mRNA were similar to the previously reported trajectories of β -actin mRNA, Levy walk interrupted by rest model might serve as a universal framework for describing the dendritic transport dynamics of mRNA irrespective of gene. Second, we observed that global inhibition of ionotropic neural activity didn't alter any of the measured kinetic parameters. This suggests that although ion input might trigger the activation of synaptic tag, instantaneous ion input from glutamatergic ionotropic receptors can be ruled out as the direct mechanism for the Arc mRNA localization to the activated synapses in the proximal dendrites. Also, this technique of imaging endogenous Arc mRNAs in real time will be served as a unique platform for finding the identity of synaptic tag which has been unknown for many years.

Several questions are remained for the future studies. First, as neuron culture and *in vivo* systems are different in many aspects, it is important to test relationship between Ca^{2+} activity and Arc transcription *in vivo*. Second, as calcium burst was induced by bicuculline, frequency or amplitude of Ca^{2+} input couldn't be controlled in this study. There might exist some optimal Ca^{2+} waveform needed for the efficient induction of Arc transcription. Third, the effect of ionotropic neural activity on Arc mRNA localization should be tested in distal dendrites. Recently there are many reports about the difference in the behaviors of cargo transport in proximal dendrite and distal dendrite. Lastly, bicuculline induces Arc transcription but bicuculline alone doesn't induce LTP. As late-LTP needs continuous supplement of newly synthesized proteins, stimulus inducing LTP might trigger more dramatic difference in the Arc mRNA transport dynamics.

Collectively, in this thesis, I first demonstrated the real-time single-molecule dynamics of endogenous Arc mRNA transcription and dendritic transport in live neurons. I could measure quantities that were impossible or extremely challenging to obtain by traditional fixed cell approaches. This innovative approach of imaging Arc mRNA in live neurons would help us elucidate the mechanism of memory consolidation by revealing its dynamic aspects.

Abstract in Korean (국문초록)

살아있는 뉴런에서의 Arc mRNA

전사과정과 움직임에 대한 연구

서울대학교 물리천문학부

물리학전공

문형석

RNA는 유전자 발현 과정에서의 중간 산물일 뿐만 아니라, 생물학적 시스템에 비대칭성을 도입하는 데에도 중요한 역할을 한다. RNA FISH (Fluorescence in situ hybridization)가 개발된 이후, 세포 내에서의 RNA솔림 현상의 다양한 역할들이 발견되었다. 특히 뇌 속에서는 시냅스 가소성과 관련 있는 여러 유전자들의 비대칭적인 발현은 기억형성에 있어서 필수적이다. 이와 관련하여 1995년에 발견된 Immediate early gene (IEG)인 *Arc* 유전자는 기억형성의 원리를 이해하는 데 큰 도움이 되었다.

Arc 유전자에게는 매우 중요한 두 가지 고유한 특성이 있다. 첫째, *Arc* 유전자의 전사과정은 강한 신경자극을 받은 후에 빠르게 일어난다. 이러한 특성으로 인해 *Arc* 유전자의 전사과정은 동물에게 행동실험을 한 후, 어느 뉴런에서 신경 활동이 있었는지 판별하는 지표로 오랫동안 사용되어 왔다. 둘째, 놀랍게도 *Arc* mRNA는 생성된 후 강한 자극을 받았던 시냅스 근처로 이동하는 것으로 밝혀졌다. 이러한 신경자극에 의

한 전사과정 개시와 신경자극을 받았던 시냅스로 모이는 특징 두 가지 모두를 가지는 유전자는 매우 드물다. 그러나 이 두 현상은 시료의 화학적 고정이 필요한 FISH 방법으로 연구되었으므로, 그 순차적 과정에 대한 정보는 얻을 수 없었다. 이 문제를 극복하기 위해, 우리는 Arc-PBS 마우스를 생성하였으며, 단일 분자 해상도로 살아있는 뉴런에서 Arc mRNA의 전사 및 이동과정을 실시간으로 촬영하는데 성공하였다.

이 논문에서 우리는 Arc 유전자의 3' 비번역부위에 반복된 PBS 서열을 삽입시킨 Arc-PBS 유전자변형 쥐를 개발하였다. RNA FISH와 웨스턴 블랏을 통해 PBS서열 삽입이 뉴런에서의 Arc mRNA양과 단백질 발현에 영향을 주지 않는 것을 확인하였다. 다음으로, 우리는 여태껏 일대일 대응 관계로 여겨졌었던 Ca^{2+} 활동과 Arc 전사활동 사이의 상관 관계를 조사하였다. 동일한 뉴런의 핵에서의 Ca^{2+} 활동과 Arc 전사과정을 처음으로 동시에 직접 측정함으로써, 해마로부터 배양한 신경세포에서는 Ca^{2+} 활동이 있었음에도 ~43 % 만이 Arc mRNA 전사과정을 개시하는 것을 관찰하였다. 또한, FISH와 면역 형광법을 함께 수행함으로써, 우리는 인산화된 CREB 단백질 양과 Arc mRNA 전사개시가 양의 상관 관계를 가짐을 관찰할 수 있었다. 이것은 Arc mRNA 전사과정을 개시하기 위한 역치 값이 뉴런마다 다를 수도 있다는 점을 제시한다. 마지막으로, 우리는 수상돌기에서 내생 Arc mRNA의 실시간 이동 과정을 단일분자 수준에서 처음으로 관찰하였다. Arc mRNA는 핵에서 멀어지는 방향과 핵으로 돌아오는 방향, 양방향으로 등속 이동하였고, 중간에 긴 멈춤 과정이 끼어 있었다. 이는 이전에 보고된 내생 β -actin mRNA의 수송 거동과 유사하였다. Arc mRNA가 신경자극을 강하게 받았던 시냅스로 쏠리는 현상을 이해하기 위해, Arc mRNA의 속도, 방향성 그리고 움직이는 비율에 대한 신경활동의 영향도 알아보았다. 놀랍게도, 이 수치들 중 어느 것도 이온 채널의 전체적인 억제에 의한 영향을 받지 않았다. 이는 Arc

mRNA는 미토콘드리아처럼 실시간 주변 이온농도에 의해서 속도를 조정하는 방식이 아닌, 다른 원리로 활성화된 시냅스로 쏠린다는 점을 시사한다.

결론적으로, 본 논문에서는 처음으로 살아있는 뉴런에서 내생 Arc mRNA의 전사과정과 수상돌기에서의 수송과정을 단일분자 수준으로 실시간 측정하였다. 이를 통해 화학적 고정을 필요로 하는 기존 방식으로는 불가능하였던 Arc mRNA의 동역학과 관련된 양들을 측정할 수 있었다. 이처럼 살아있는 뉴런에서 Arc mRNA의 실시간 동역학을 관찰하는 혁신적인 방법은 기존 방식들로는 접근할 수 없었던 기억형성 과정의 원리를 밝히는 데 큰 기여를 할 것으로 기대된다.

핵심어: Arc mRNA, 전사, RNA 쏠림 현상, 수상돌기내 운송과정, 단분자촬영, 살아있는 세포에서의 촬영

학번: 2014-22365